Chapter 4. Plastic Yield Criterion (Hencky-Mises Failure Criterion) and How Its Interaction with Spatially Heterogeneous Stress Biases Earthquake Failures Toward the Stress Rate Tensor, $\dot{\boldsymbol{\sigma}}'_T$

Overview of Why Understanding the Fracture Criterion Is Important

In this chapter we wish to demonstrate that as the amplitude of the heterogeneity increases, the orientations of the failures in our simulations become increasingly biased toward the stress rate tensor, $\dot{\boldsymbol{\sigma}}'_T$. We will do this by 1) analyzing the fracture criterion used to bring points to failure as synthetic earthquakes and 2) examining P-T plots of synthetic focal mechanisms from our simulations.

If the real Earth has significant spatially heterogeneous stress, which we have reason to believe it does, our observation of bias toward the stress rate, $\dot{\boldsymbol{\sigma}}'_T$, has important implications for interpreting stress inversion studies. Currently, it is assumed that the popularly used stress inversion schemes [*Angelier*, 1975; 1984; *Carey and Brunier*, 1974; *Etchecopar, et al.*, 1981; *Gephart*, 1990; *Gephart and Forsyth*, 1984; *Mercier and Carey-Gailhardis*, 1989; *Michael*, 1984; 1987] measure the spatially uniform component of the tectonic stress tensor, which we call $\boldsymbol{\sigma}'_B$ (the background stress). If the Earth also experiences a bias toward the $\dot{\boldsymbol{\sigma}}'_T$ in the presence of spatially heterogeneous stress as seen in our simulations, then this bias must be subtracted to correctly estimate $\boldsymbol{\sigma}'_B$. If the heterogeneity has too large of an amplitude, the correction may be possible, and one will not be able to determine $\boldsymbol{\sigma}'_B$. An outline of how one might begin to subtract out this $\dot{\boldsymbol{\sigma}}'_T$ bias and determine $\boldsymbol{\sigma}'_B$ is presented in Chapter 5. In any case, our simulation results imply that one must be very careful in interpreting stress inversion results, as they may be more complicated than commonly assumed.

In the real Earth, stress inversion schemes are commonly used to infer deviatoric stress information from focal mechanism orientations. In particular, the three principal deviatoric stress axes orientations are calculated along with a dimensionless quantity that relates the magnitudes of the principal stresses, the stress ratio, $R = \left(\frac{\sigma_2 - \sigma_3}{\sigma_1 - \sigma_3} \right)$ [e.g., *Rivera and Kanamori*, 2002]. In this study we are not addressing whether or not the stress inversion schemes accurately invert the given focal mechanism data. Instead, we are questioning an assumption that goes into the interpretation of the results. The implicit assumption we question is, "Focal mechanisms are a good uniform random measurement of stress in the Earth's crust." In other words, "the points which fail and produce earthquake focal mechanisms uniformly sample the actual stress field, and upon inversion, yield the spatial mean stress tensor, $\boldsymbol{\sigma}'_B$." In our simulations, we show that the interaction of the failure criterion with spatially heterogeneous stress produces a bias to which orientations and stress ratios, R, are most likely to fail, a bias toward our stress rate tensor, $\dot{\boldsymbol{\sigma}}'_T$. If this is indicative of the real Earth, then the answer to our question would be no, focal mechanism data sets are not a good uniform random sampler of stress. Not all points fail in the real Earth as earthquakes in a regional stress study, only a minute fraction. The points that are most likely to fail will be those aligned with $\dot{\boldsymbol{\sigma}}'_T$; hence, the set of focal mechanisms included in inversion studies will produce an inverted stress tensor biased toward $\dot{\boldsymbol{\sigma}}'_T$. See Figure 4.1 for a simple scalar example of bias to visually demonstrate this concept.

In Figure 4.1 we show a scalar quantity represented by the length of the vertical bars. Set A represents the entire data set and Set B is the first half of the data. The scalar

quantities have been arranged so that the larger values happen first and cluster in Set B. Because the larger values occur first, estimates of the scalar value will be biased if they use only the first half of the data set, Set B. Similarly, we ask, could the focal mechanisms used in standard stress inversions be a biased sampling of stress in the real Earth? Only a small fraction of all the possible points in a study region fail within the study window when applying stress inversions, and there is the possibility that this small subset of all possible points could have a biased average orientation. If so, interpretations of stress inversions may need to be revised. This is a difficult question to answer by observation alone, which is why we numerically investigate this problem.

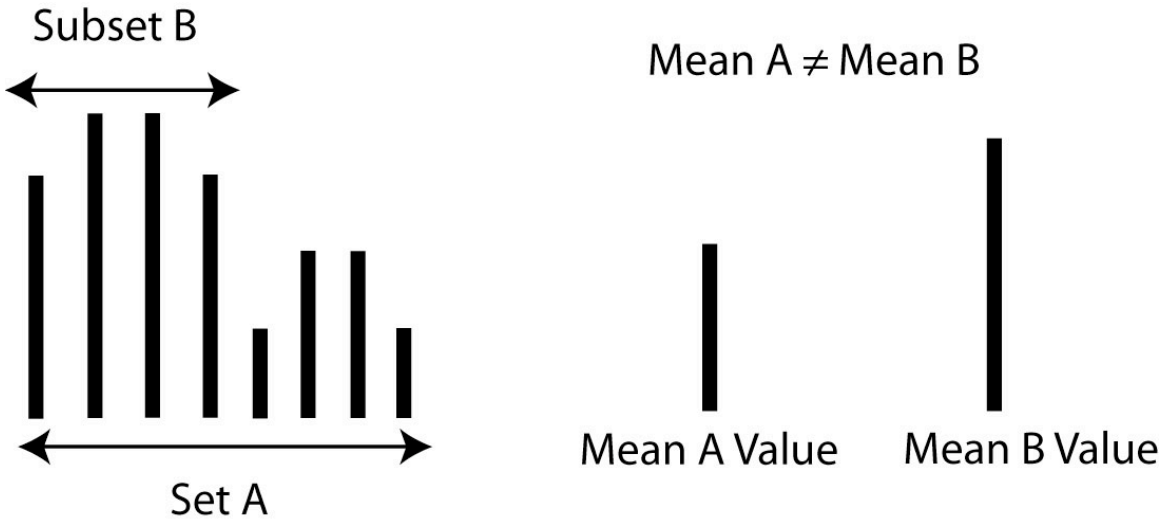

Figure 4.1. *This is a simple scalar example of bias. The entire data set is represented by Set A. The first half of the data set is represented by Set B. In this case, the larger values happen first and cluster in Set B. One cannot estimate the mean of Set A by measuring only Set B, because of the bias towards larger scalar values in Set B. Similarly, if there is a bias in which points fail as earthquakes, produce focal mechanisms, and are included in stress inversion studies, then the results of stress inversion studies may also be biased; consequently, stress inversion studies may not reflect the spatial mean stress as commonly assumed.*

Fracture Criterion Used to Produce Earthquakes—Hencky-Mises Plastic Yield

The Hencky-Mises plastic yield condition [*Housner and Vreeland*, 1965] is the preferred fracture criterion for this thesis because of its simplicity. It predicts failure when the maximum shear stress is greater than a threshold value. The measure used is an invariant quantity so this failure criterion works regardless of the coordinate system or orientation of the individual stress tensors. The coefficient of friction is essentially zero (optimally oriented planes) and pressure does not enter into the equation. (If one wishes to investigate non-zero pressures and coefficients of friction see Appendix C, Coulomb Fracture Criterion.) Last, because we are dealing with optimally oriented planes, the conjugate planes become mathematically indistinguishable. The equation for this plastic yield is

$$I_2' = \frac{2}{3}\tau_0^2 \tag{4.1}$$

[*Housner and Vreeland*, 1965] where τ_0 is the uniaxial yield stress and I_2' is the second invariant of the deviatoric stress tensor, $\boldsymbol{\sigma}'$, where

$$I_2' = \sigma_{11}'^2 + \sigma_{22}'^2 + \sigma_{33}'^2 + 2\left[\sigma_{12}'^2 + \sigma_{23}'^2 + \sigma_{13}'^2\right]. \tag{4.2}$$

At this point it is useful to introduce the tensor scalar product to aid us in our equation derivations. The scalar product of two tensors, A and B, can be defined as

$$A : B = \sum_{i=1}^{3}\sum_{j=1}^{3} A_{ij}B_{ij}. \tag{4.3}$$

In this notation the second invariant of the deviatoric stress tensor can now be written as,

$$I_2' = \boldsymbol{\sigma}' : \boldsymbol{\sigma}', \tag{4.4}$$

which is a much more compact notation.

In our simulations, we wish to determine when each individual point in the 3D grid fails; hence, we are interested in examining the failure equation for each single spatial grid point, $\mathbf{x}_i$, where $\mathbf{x}_i$ is the 3D coordinate of the ith point in the grid. The equation for a single point is

$$I_2'(\mathbf{x}_i,t) = \boldsymbol{\sigma}'(\mathbf{x}_i,t) : \boldsymbol{\sigma}'(\mathbf{x}_i,t). \tag{4.5}$$

It is the summation of the squared deviatoric stress matrix elements. If our deviatoric stress tensor at any point in the grid is

$$\boldsymbol{\sigma}'(\mathbf{x}_i,t) = \boldsymbol{\sigma}'_H(\mathbf{x}_i) + \boldsymbol{\sigma}'_B + \dot{\boldsymbol{\sigma}}'_T\ t \tag{4.6}$$

where $\boldsymbol{\sigma}'_H(\mathbf{x}_i)$ is the spatially heterogeneous stress, $\boldsymbol{\sigma}'_B$ is the spatially and temporally uniform background tectonic stress, and $\dot{\boldsymbol{\sigma}}'_T\ t$ is the linearly increasing secular component of tectonic stress from plate motion, then our failure criterion can be rewritten as

$$I_2'(\mathbf{x}_i,t) = \left(\boldsymbol{\sigma}'_H(\mathbf{x}_i) + \boldsymbol{\sigma}'_B + \dot{\boldsymbol{\sigma}}'_T\ t\right) : \left(\boldsymbol{\sigma}'_H(\mathbf{x}_i) + \boldsymbol{\sigma}'_B + \dot{\boldsymbol{\sigma}}'_T\ t\right). \tag{4.7}$$

Multiplying through, we have

$$\begin{aligned} I_2'(\mathbf{x}_i,t) = {} & \boldsymbol{\sigma}'_H(\mathbf{x}_i) : \boldsymbol{\sigma}'_H(\mathbf{x}_i) + \boldsymbol{\sigma}'_B : \boldsymbol{\sigma}'_B + \left(\dot{\boldsymbol{\sigma}}'_T : \dot{\boldsymbol{\sigma}}'_T\right) t^2 \\ & + 2\boldsymbol{\sigma}'_H(\mathbf{x}_i) : \boldsymbol{\sigma}'_B + 2\boldsymbol{\sigma}'_H(\mathbf{x}_i) : \dot{\boldsymbol{\sigma}}'_T\ t + 2\boldsymbol{\sigma}'_B : \dot{\boldsymbol{\sigma}}'_T\ t. \end{aligned} \tag{4.8}$$

Note that

$$\left(\boldsymbol{\sigma}'_H(\mathbf{x}_i) + \boldsymbol{\sigma}'_B\right) : \left(\boldsymbol{\sigma}'_H(\mathbf{x}_i) + \boldsymbol{\sigma}'_B\right) = \boldsymbol{\sigma}'_H(\mathbf{x}_i) : \boldsymbol{\sigma}'_H(\mathbf{x}_i) + 2\boldsymbol{\sigma}'_H(\mathbf{x}_i) : \boldsymbol{\sigma}'_B + \boldsymbol{\sigma}'_B : \boldsymbol{\sigma}'_B \tag{4.9}$$

and

$$2\left(\boldsymbol{\sigma}'_H(\mathbf{x}_i) + \boldsymbol{\sigma}'_B\right) : \dot{\boldsymbol{\sigma}}'_T\ t = 2\boldsymbol{\sigma}'_H(\mathbf{x}_i) : \dot{\boldsymbol{\sigma}}'_T\ t + 2\boldsymbol{\sigma}'_B : \dot{\boldsymbol{\sigma}}'_T\ t. \tag{4.10}$$

Therefore, we can rewrite our second invariant as

$$I_2'(\mathbf{x}_i,t) = \left(\boldsymbol{\sigma}_H'(\mathbf{x}_i) + \boldsymbol{\sigma}_B'\right) : \left(\boldsymbol{\sigma}_H'(\mathbf{x}_i) + \boldsymbol{\sigma}_B'\right) + \left(\dot{\boldsymbol{\sigma}}_T' : \dot{\boldsymbol{\sigma}}_T'\right)t^2 + 2\left(\boldsymbol{\sigma}_H'(\mathbf{x}_i) + \boldsymbol{\sigma}_B'\right) : \dot{\boldsymbol{\sigma}}_T'\ t. \tag{4.11}$$

Interestingly, the first term is simply the second invariant of the deviatoric stress tensor at time $t = 0$. This means we can write our equation as

$$I_2'(\mathbf{x}_i,t) = I_2'(\mathbf{x}_i,0) + \left(\dot{\boldsymbol{\sigma}}_T' : \dot{\boldsymbol{\sigma}}_T'\right)t^2 + 2\left(\boldsymbol{\sigma}_H'(\mathbf{x}_i) + \boldsymbol{\sigma}_B'\right) : \dot{\boldsymbol{\sigma}}_T'\ t \tag{4.12}$$

where

$$I_2'(\mathbf{x}_i,0) = \left(\boldsymbol{\sigma}_H'(\mathbf{x}_i) + \boldsymbol{\sigma}_B'\right) : \left(\boldsymbol{\sigma}_H'(\mathbf{x}_i) + \boldsymbol{\sigma}_B'\right). \tag{4.13}$$

We now ask, at what time, t_F, does $I_2' = \frac{2}{3}\tau_0^2$, for each point $\mathbf{x}_i$, where t_F is the time of failure? To address this question conceptually, we can divide $I_2'(\mathbf{x}_i,t)$ into three components,

$$I_2'(\mathbf{x}_i,t) = I_2'(\mathbf{x}_i,0) + \frac{dI_2'(\mathbf{x}_i,t)}{dt}t - \left(\dot{\boldsymbol{\sigma}}_T' : \dot{\boldsymbol{\sigma}}_T'\right)t^2 \tag{4.14}$$

where

$$\frac{dI_2'(\mathbf{x}_i,t)}{dt} = 2\left(\dot{\boldsymbol{\sigma}}_T' : \dot{\boldsymbol{\sigma}}_T'\right)t + 2\left(\boldsymbol{\sigma}_H'(\mathbf{x}_i) + \boldsymbol{\sigma}_B'\right) : \dot{\boldsymbol{\sigma}}_T'. \tag{4.15}$$

For small stressing rates, $\dot{\boldsymbol{\sigma}}_T'$, and small times, t (which will be true for the simulations shown), all the $\left(\dot{\boldsymbol{\sigma}}_T' : \dot{\boldsymbol{\sigma}}_T'\right)t$ terms are ≈ 0.

Therefore, we have two main terms,

$$I_2'(\mathbf{x}_i,t) \approx I_2'(\mathbf{x}_i,0) + \frac{dI_2'(\mathbf{x}_i,t)}{dt}t \tag{4.16}$$

where

$$I_2'(\mathbf{x}_i,0) = \left(\boldsymbol{\sigma}_H'(\mathbf{x}_i) + \boldsymbol{\sigma}_B'\right) : \left(\boldsymbol{\sigma}_H'(\mathbf{x}_i) + \boldsymbol{\sigma}_B'\right) \tag{4.17}$$

and

$$\frac{dI_2'(\mathbf{x}_i,t)}{dt} \approx 2\left(\boldsymbol{\sigma}_H'(\mathbf{x}_i) + \boldsymbol{\sigma}_B'\right) : \dot{\boldsymbol{\sigma}}_T'. \tag{4.18}$$

The first term of equation (4.16), $I_2'(\mathbf{x}_i,0)$, shows the state of the system at $t = 0$ and the heterogeneity of the system. The second term, $\frac{dI_2'(\mathbf{x}_i,t)}{dt}$, describes how quickly points are either increasing or decreasing their maximum deviatoric shear stress. For a point to fail quickly, it generally needs to satisfy the following three criteria.

- $I_2'(\mathbf{x}_i,0) < \frac{2}{3}\tau_0^2$. In other words, the point $\mathbf{x}_i$, at $t = 0$, must have an I_2' less than the the failure threshold of $\frac{2}{3}\tau_0^2$, to be considered in the simulation. We find that the placement of the failure threshold, $\frac{2}{3}\tau_0^2$, determines what part of the heterogeneity we sample; i.e., do we place $\frac{2}{3}\tau_0^2$ above the maximum $I_2'(\mathbf{x}_i,0)$ and sample extreme outliers that would have already plastically yielded, or do we place the failure threshold at the 1.5–2.0 standard deviation level within $I_2'(\mathbf{x}_i,0)$ and exclude the top 5–15% of the points as outliers?

- $\dfrac{\frac{2}{3}\tau_0^2 - I_2'(\mathbf{x}_i,0)}{\frac{2}{3}\tau_0^2} \ll 1$. For a point $\mathbf{x}_i$ to fail quickly and be considered in the first 2,000 failures of the simulations, it needs to start with a value of $I_2'(\mathbf{x}_i,0)$ quite close to the failure threshold, $\frac{2}{3}\tau_0^2$, at $t = 0$.

- $\dfrac{dI_2'(\mathbf{x}_i,t)}{dt} > 0$, and preferably maximized. The time derivative of $I_2'(\mathbf{x}_i,t)$ must be greater than zero if there is to be any failure at all. If $I_2'(\mathbf{x}_i,0) < \frac{2}{3}\tau_0^2$ and $\dfrac{dI_2'(\mathbf{x}_i,t)}{dt} > 0$ then the point $\mathbf{x}_i$ is progressing toward the failure threshold $\frac{2}{3}\tau_0^2$. If $I_2'(\mathbf{x}_i,0) < \frac{2}{3}\tau_0^2$ and $\dfrac{dI_2'(\mathbf{x}_i,t)}{dt} < 0$ the point $\mathbf{x}_i$ is moving further away from the failure threshold $\frac{2}{3}\tau_0^2$. Obviously, the larger the positive rate of change, $\dfrac{dI_2'(\mathbf{x}_i,t)}{dt}$, the more quickly $\mathbf{x}_i$ progesses toward failure.

Placement of the Failure Threshold

We opt to normalize $I_2'(\mathbf{x}_i,0)$ so that the failure threshold $\frac{2}{3}\tau_0^2$ falls somewhat below the maximum $I_2'(\mathbf{x}_i,0)$ value to avoid outliers for several reasons: 1) The points with largest values of $I_2'(\mathbf{x}_i,0)$ would already have plastically failed. 2) Sampling the extreme outliers in the simulations results in non-steady earthquake rates. There are very few events at first, as one samples the extreme outliers, then the rate rapidly accelerates

as one begins to sample the rest of the heterogeneity. Normalizing $I_2'(\mathbf{x}_i,0)$ so that $\frac{2}{3}\tau_0^2$ falls at 1.5 or 2.0 standard deviations produces relatively constant earthquake rates over 4 orders of magnitude in time. 3) The distribution of tensors present in the family of heterogeneous stress tensors, $\boldsymbol{\sigma}'_H(\mathbf{x}_i)$, with values of $I_2'(\mathbf{x}_i,0)$ close to the failure threshold, $\frac{2}{3}\tau_0^2$, partially depends on where the failure threshold falls within the $I_2'(\mathbf{x}_i,0)$ distribution. If $\frac{2}{3}\tau_0^2$ = *Maximum* $I_2'(\mathbf{x}_i,0)$, then all the points close to $\frac{2}{3}\tau_0^2$ will have $\boldsymbol{\sigma}'_H(\mathbf{x}_i) \approx \boldsymbol{\sigma}'_B$. If $\frac{2}{3}\tau_0^2$ falls at the 1.5 or 2.0 standard deviation level for $I_2'(\mathbf{x}_i,0)$ (i.e. excluding the top ~ 15% or ~ 5% points in $I_2'(\mathbf{x}_i,0)$ respectively), there is still bias toward $\boldsymbol{\sigma}'_B$, but there is generally a greater variety of $\boldsymbol{\sigma}'_H(\mathbf{x}_i)$ that produce $\frac{\frac{2}{3}\tau_0^2 - I_2'(\mathbf{x}_i,0)}{\frac{2}{3}\tau_0^2} \ll 1$. If $\frac{2}{3}\tau_0^2$ falls at the 1.5 standard deviations level for $I_2'(\mathbf{x}_i,0)$ or less, we start throwing out too many points associated with the $\boldsymbol{\sigma}'_B$ orientation, and a hole appears right at the $\boldsymbol{\sigma}'_B$ orientation in our P-T plots.

On the other hand, if $I_2'(\mathbf{x}_i,0)$ is normalized so that $\frac{2}{3}\tau_0^2$ falls at the 2.0 standard deviation level for $I_2'(\mathbf{x}_i,0)$, with 95% of the points in $I_2'(\mathbf{x}_i,0)$ below the failure threshold, we find a satisfactory tradeoff. Simulations with this normalization of $I_2'(\mathbf{x}_i,0)$ have fairly steady earthquake rates over several orders of magnitude in time and still provide a good variety of $\boldsymbol{\sigma}'_H(\mathbf{x}_i)$ close to and aligned with $\boldsymbol{\sigma}'_B$.

Plots of $I_2'(x_i,0)$ with units of $\left[Stress^2\right]$ and the failure threshold, $\frac{2}{3}\tau_0^2$, in 1D are shown in Figure 4.2 for four different values of spatial smoothing, $\alpha = 0.0, 0.5, 1.0,$ and 1.5. Within each plot, $I_2'(x_i,0)$ is shown for three different values of the Heterogeneity Ratio, $HR = \frac{\sqrt{Mean\left[\ \boldsymbol{\sigma}'_H(\mathbf{x}_i) : \boldsymbol{\sigma}'_H(\mathbf{x}_i)\right]}}{\sqrt{\boldsymbol{\sigma}'_B : \boldsymbol{\sigma}'_B}}$, where $\boldsymbol{\sigma}'_H(\mathbf{x}_i) : \boldsymbol{\sigma}'_H(\mathbf{x}_i)$ is the second invariant of the heterogeneous stress tensor, $\boldsymbol{\sigma}'_H(\mathbf{x}_i)$, and $\boldsymbol{\sigma}'_B : \boldsymbol{\sigma}'_B$ is the second invariant of the spatially homogeneous, background stress tensor, $\boldsymbol{\sigma}'_B$. In order of increasing heterogeneity amplitude, we have $HR = 0.1$ plotted in red, $HR = 0.3$ plotted in green, and $HR = 1.0$ plotted in blue. They have been normalized so that 95% of the points fall below the same failure threshold level, $\frac{2}{3}\tau_0^2$, the $I_2'(x_i,0)$ 2.0 standard deviation level. $\frac{2}{3}\tau_0^2$ is plotted with the thick, horizontal, dashed, black line. The main points we wish to show are simply that 1) as HR increases, the heterogeneous amplitude $I_2'(x_i,0)$ increases, 2) as α increases, the spatial smoothing of $I_2'(x_i,0)$ increases.

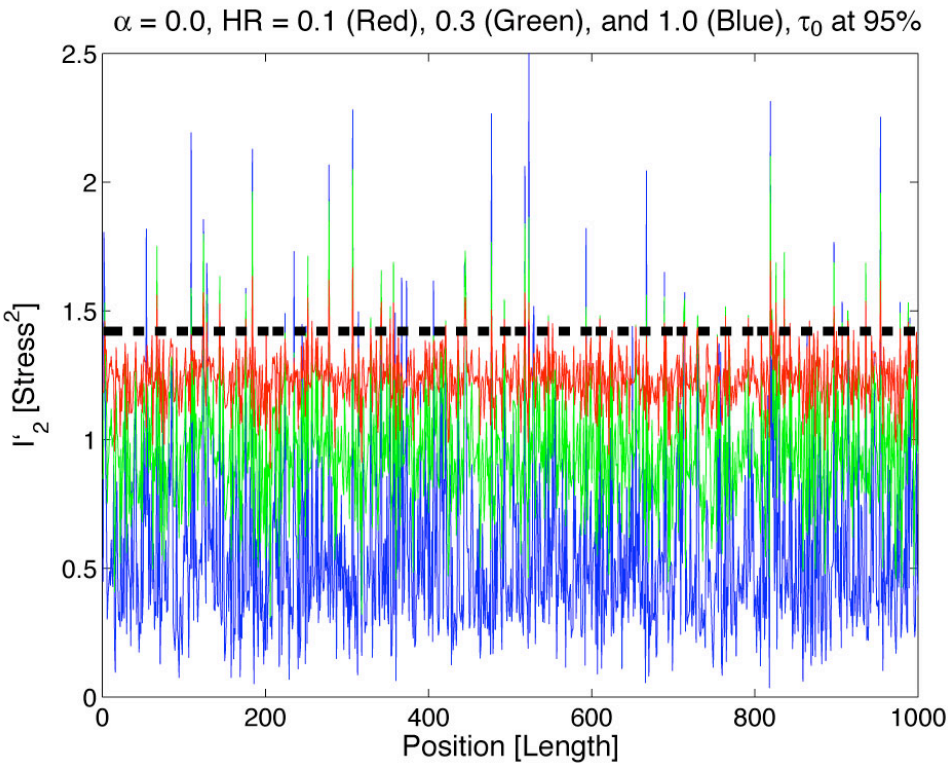

Figure 4.2 a)

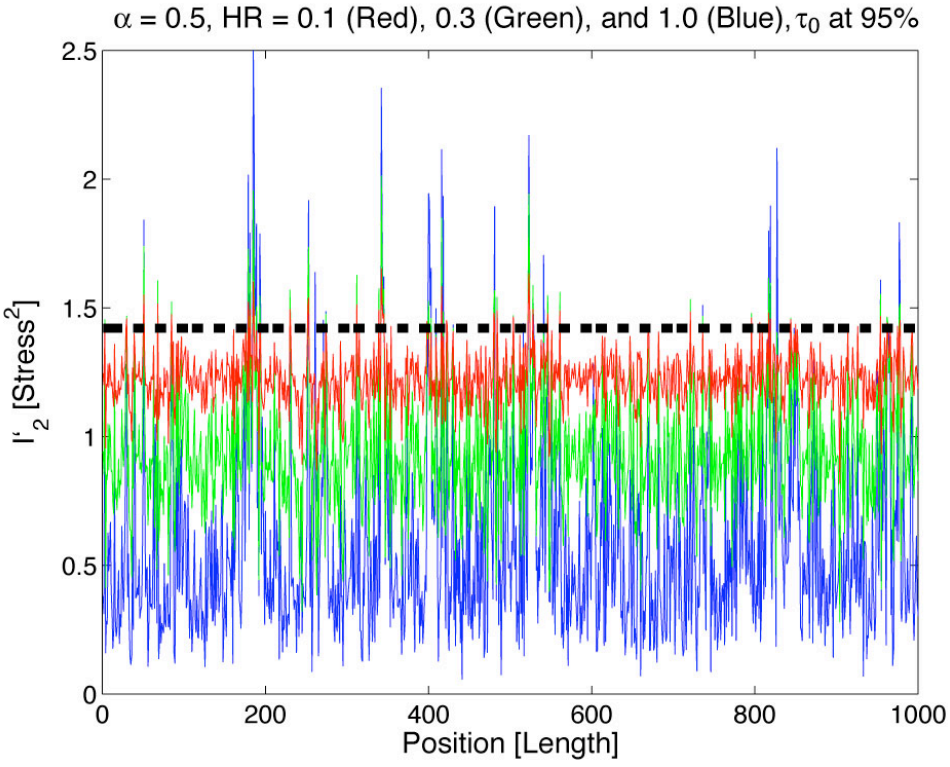

Figure 4.2 b)

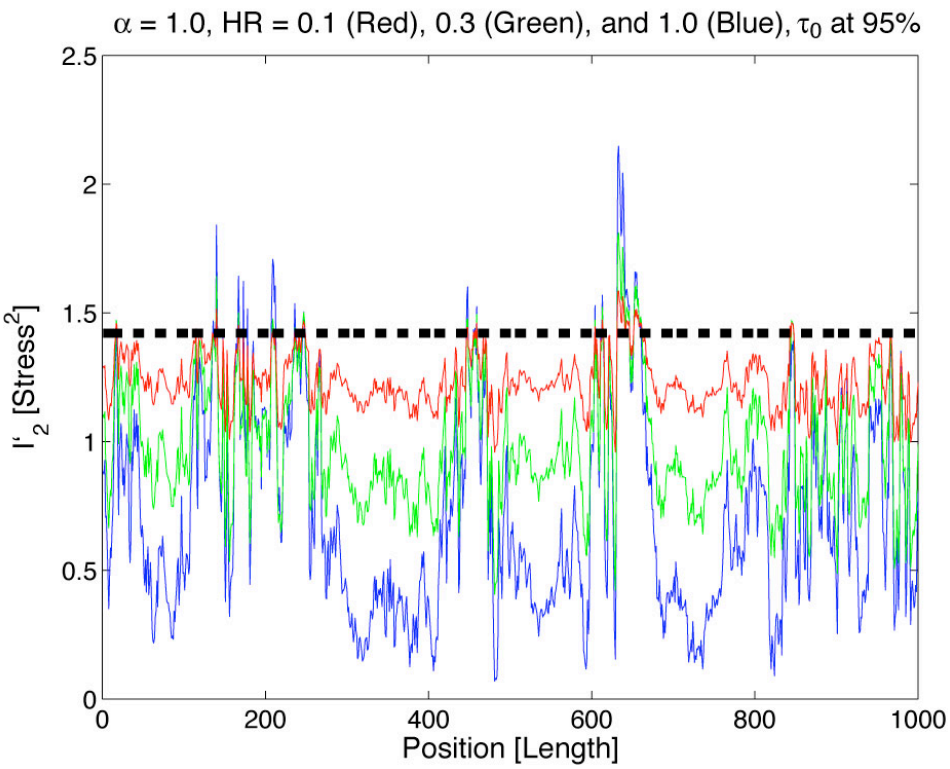

Figure 4.2 c)

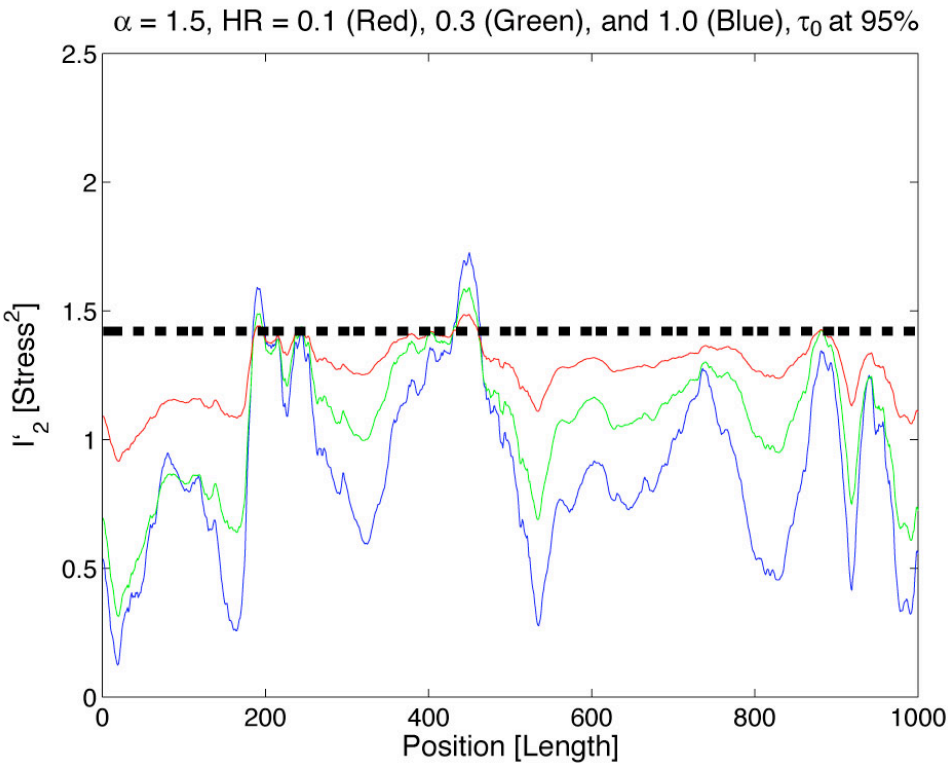

Figure 4.2 d)

Figure 4.2. *Plots of* $I_2'(x_i,0)$ *for 1,001 points in 1D, to show what the maximum shear stress looks like at* $t=0.0$. *To create* $I_2'(x_i,0)$, *we generate* $\boldsymbol{\sigma}'_H(x_i)$ *with different levels of spatial filtering,* ***a)*** $\alpha=0.0$, ***b)*** $\alpha=0.5$, ***c)*** $\alpha=1.0$, *and* ***d)*** $\alpha=1.5$, *and add it component-wise to a background stress tensor,* $\boldsymbol{\sigma}'_B$, *using three different heterogeneous amplitudes within each plot. Within each plot, we have* $HR=0.1$ *in red,* $HR=0.3$ *in green, and* $HR=1.0$ *in blue.* $I_2'(x_i,0)$ *is normalized so that the failure threshold,* $\frac{2}{3}\tau_0^2$, *the thick, dashed, black line, falls at the 2.0 standard deviation level of* $I_2'(x_i,0)$ *values. This means approximately 95% of the values of* $I_2'(x_i,0)$ *are below* $\frac{2}{3}\tau_0^2$. *Any points below* $\frac{2}{3}\tau_0^2$ *can be counted as failures in the simulation, and any points above* $\frac{2}{3}\tau_0^2$ *at time* $t=0$ *are considered outliers that have previously plastically failed. The points that are most likely to fail first are those that have* $I_2'(x_i,0)$ *close to the failure threshold,* $\frac{2}{3}\tau_0^2$, *i.e.,* $\frac{\frac{2}{3}\tau_0^2 - I_2'(\mathbf{x}_i,0)}{\frac{2}{3}\tau_0^2} \ll 1$, *and are quickly moving toward failure, i.e.,* $\frac{dI_2'(\mathbf{x}_i,t)}{dt}$ *large and positive.*

Why the Most Likely Points to Fail Are Biased Toward $\dot{\boldsymbol{\sigma}}'_T$, When the Heterogeneity Ratio, *HR*, Is Large

To understand why we have an increasing bias toward $\dot{\boldsymbol{\sigma}}'_T$ as the heterogeneous ratio, HR (a measure of the heterogeneity amplitude), increases, we once more look at equation (4.16), $I'_2(\mathbf{x}_i,t) \approx I'_2(\mathbf{x}_i,0) + \dfrac{dI'_2(\mathbf{x}_i,t)}{dt}t$. We rewrite the first and second terms. The first term on the right hand side, $I'_2(\mathbf{x}_i,0)$, which describes the initial stress state, can be rewritten as

$$I'_2(x_i,0) = \boldsymbol{\sigma}'_H(\mathbf{x}_i) : \boldsymbol{\sigma}'_H(\mathbf{x}_i) + 2\boldsymbol{\sigma}'_H(\mathbf{x}_i) : \boldsymbol{\sigma}'_B + \boldsymbol{\sigma}'_B : \boldsymbol{\sigma}'_B \tag{4.19}$$

or

$$I'_2(x_i,0) = \boldsymbol{\sigma}'_H(\mathbf{x}_i) : \boldsymbol{\sigma}'_H(\mathbf{x}_i) + 2\boldsymbol{\sigma}'_H(\mathbf{x}_i) : \boldsymbol{\sigma}'_B + C_0 \tag{4.20}$$

where the constant

$$C_0 = \boldsymbol{\sigma}'_B : \boldsymbol{\sigma}'_B. \tag{4.21}$$

The second term on the right hand side of equation (4.16), $\dfrac{dI'_2(\mathbf{x}_i,t)}{dt}$, which describes whether or not the points are going toward failure, can be rewritten as,

$$\frac{dI'_2(\mathbf{x}_i,t)}{dt} \approx 2\boldsymbol{\sigma}'_H(\mathbf{x}_i) : \dot{\boldsymbol{\sigma}}'_T + 2\boldsymbol{\sigma}'_B : \dot{\boldsymbol{\sigma}}'_T \tag{4.22}$$

or

$$\frac{dI'_2(\mathbf{x}_i,t)}{dt} \approx 2\boldsymbol{\sigma}'_H(\mathbf{x}_i) : \dot{\boldsymbol{\sigma}}'_T + C_1 \tag{4.23}$$

where the constant is

$$C_1 = 2\boldsymbol{\sigma}'_B : \dot{\boldsymbol{\sigma}}'_T. \tag{4.24}$$

Since C_1 is a constant, it has the same value at every point $\mathbf{x}_i$ and C_1 simply determines when $\frac{dI_2'(\mathbf{x}_i,t)}{dt} > 0$. For example, if $\dot{\boldsymbol{\sigma}}_T' = -c\,\boldsymbol{\sigma}_B'$, where c is a constant, we will have $C_1 < 0$, and a number of points will now go away from failure instead of toward it. If the heterogeneity is sufficiently small, $HR << 1$, and $C_1 < 0$, we may find there are no failures right away. Determining the set of points that have $\frac{dI_2'(\mathbf{x}_i,t)}{dt} > 0$ is the main effect of C_1, but because it is a constant, we can ignore it when assessing which points are more likely to fail than others; instead, we need to primarily look at the terms that are a function of $\mathbf{x}_i$, to determine why the failures are biased toward $\dot{\boldsymbol{\sigma}}_T'$.

The term that is a function of $\mathbf{x}_i$ in $\frac{dI_2'(\mathbf{x}_i,t)}{dt}$ is $2\boldsymbol{\sigma}_H'(\mathbf{x}_i) : \dot{\boldsymbol{\sigma}}_T'$. Because it involves component-wise cross-terms of the heterogeneous stress tensor, $\boldsymbol{\sigma}_H'(\mathbf{x}_i)$, and the stress rate tensor, $\dot{\boldsymbol{\sigma}}_T'$, we predict that the points that have the largest, positive $\frac{dI_2'(\mathbf{x}_i,t)}{dt}$ will be those where $\boldsymbol{\sigma}_H'(\mathbf{x}_i)$ is on average aligned component-wise with $\dot{\boldsymbol{\sigma}}_T'$.

What about $I_2'(x_i,0)$? How does this affect which points are most likely to fail? Examining equations (4.20) and (4.21), we see that the value of the constant C_0 simply raises or lowers all the points in $I_2'(x_i,0)$; it has no bearing on which points are most likely to fail, because we normalize the overall size of $I_2'(x_i,0)$, so that the 95% level is at the failure threshold, $\frac{2}{3}\tau_0^2$. Now the other two terms in equation (4.20) are more interesting because they do have different values as a function of $\mathbf{x}_i$. $2\boldsymbol{\sigma}_H'(\mathbf{x}_i) : \boldsymbol{\sigma}_B'$

involves component-wise cross terms between the heterogeneous stress, $\boldsymbol{\sigma}'_H(\mathbf{x}_i)$, and the background stress, $\boldsymbol{\sigma}'_B$; therefore, this term will tend to promote points with $\boldsymbol{\sigma}'_H(\mathbf{x}_i)$ on average aligned with $\boldsymbol{\sigma}'_B$ to be near the failure threshold. However, there is one more term to consider, $\boldsymbol{\sigma}'_H(\mathbf{x}_i):\boldsymbol{\sigma}'_H(\mathbf{x}_i)$, which is simply the second invariant of $\boldsymbol{\sigma}'_H(\mathbf{x}_i)$. $\boldsymbol{\sigma}'_H(\mathbf{x}_i):\boldsymbol{\sigma}'_H(\mathbf{x}_i)$ promotes points to be near the failure criterion if the overall size of $\boldsymbol{\sigma}'_H(\mathbf{x}_i)$ is large irrespective of orientation. Consequently, if $\boldsymbol{\sigma}'_H(\mathbf{x}_i):\boldsymbol{\sigma}'_H(\mathbf{x}_i) >> 2\boldsymbol{\sigma}'_H(\mathbf{x}_i):\boldsymbol{\sigma}'_B$, then there will be little to no bias to which $\boldsymbol{\sigma}'_H(\mathbf{x}_i)$ orientations are close to the threshold, and the $2\boldsymbol{\sigma}'_H(\mathbf{x}_i):\dot{\boldsymbol{\sigma}}'_T$ term will primarily choose points to fail where $\boldsymbol{\sigma}'_H(\mathbf{x}_i)$ is on average aligned with $\dot{\boldsymbol{\sigma}}'_T$. Now if $\boldsymbol{\sigma}'_H(\mathbf{x}_i):\boldsymbol{\sigma}'_H(\mathbf{x}_i) << 2\boldsymbol{\sigma}'_H(\mathbf{x}_i):\boldsymbol{\sigma}'_B$, we expect the bias in $\boldsymbol{\sigma}'_H(\mathbf{x}_i)$ toward $\boldsymbol{\sigma}'_B$ to be significant for points near the failure threshold.

Another way to quantify this is in terms of the Heterogeneity Ratio, $HR = \dfrac{\sqrt{Mean\left[\ \boldsymbol{\sigma}'_H(\mathbf{x}_i):\boldsymbol{\sigma}'_H(\mathbf{x}_i)\right]}}{\sqrt{\boldsymbol{\sigma}'_B:\boldsymbol{\sigma}'_B}}$, where if $HR << 1$, $\boldsymbol{\sigma}'_H(\mathbf{x}_i):\boldsymbol{\sigma}'_H(\mathbf{x}_i) << 2\boldsymbol{\sigma}'_H(\mathbf{x}_i):\boldsymbol{\sigma}'_B$, and the $\boldsymbol{\sigma}'_{H_{Failure}}\left(\mathbf{x}_{i_{Failure}}\right)$ (the heterogeneous stress of those points that fail) will be biased toward the $\boldsymbol{\sigma}'_B$. As HR increases, $\boldsymbol{\sigma}'_{H_{Failure}}\left(\mathbf{x}_{i_{Failure}}\right)$ will be decreasingly biased toward $\boldsymbol{\sigma}'_B$ and increasingly biased toward $\dot{\boldsymbol{\sigma}}'_T$, until as $HR >> 1$, $\boldsymbol{\sigma}'_H(\mathbf{x}_i):\boldsymbol{\sigma}'_H(\mathbf{x}_i) >> 2\boldsymbol{\sigma}'_H(\mathbf{x}_i):\boldsymbol{\sigma}'_B$, and $\bar{\boldsymbol{\sigma}}'_{H_{Failure}}\left(\mathbf{x}_{i_{Failure}}\right) \approx \dot{\boldsymbol{\sigma}}'_T$.

Now that we have examined how the failure criterion, $I'_2(\mathbf{x}_i,t) = \dfrac{2}{3}\tau_0^2$, affects the selection of $\boldsymbol{\sigma}'_{H_{Failure}}\left(\mathbf{x}_{i_{Failure}}\right)$, biasing it toward $\boldsymbol{\sigma}'_B$ for $HR << 1$ and toward $\dot{\boldsymbol{\sigma}}'_T$ for

$HR >> 1$, keep in mind that the final stress tensor at failure is a summation of three terms, $\boldsymbol{\sigma}'_{Failure}\left(\mathbf{x}_{i_{Failure}}, t_{Failure}\right) = \boldsymbol{\sigma}'_{H_{Failure}}\left(\mathbf{x}_{i_{Failure}}\right) + \boldsymbol{\sigma}'_B + \dot{\boldsymbol{\sigma}}'_T\ t$. For small, $\dot{\boldsymbol{\sigma}}'_T\ t$, the orientation of our failure stress tensors are primarily a tradeoff between $\boldsymbol{\sigma}'_{H_{Failure}}\left(\mathbf{x}_{i_{Failure}}\right)$ and $\boldsymbol{\sigma}'_B$. If $HR << 1$, $\boldsymbol{\sigma}'_{Failure}\left(\mathbf{x}_{i_{Failure}}, t_{Failure}\right) \approx \boldsymbol{\sigma}'_B$, and if $HR >> 1$, $\boldsymbol{\sigma}'_{Failure}\left(\mathbf{x}_{i_{Failure}}, t_{Failure}\right) \approx \boldsymbol{\sigma}'_{H_{Failure}}\left(\mathbf{x}_{i_{Failure}}\right)$.

In summary:

- If $HR << 1$
  - $\bar{\boldsymbol{\sigma}}'_{H_{Failure}}\left(\mathbf{x}_{i_{Failure}}\right)$ biased toward $\boldsymbol{\sigma}'_B$.
  - $\boldsymbol{\sigma}'_{Failure}\left(\mathbf{x}_{i_{Failure}}, t_{Failure}\right) \approx \boldsymbol{\sigma}'_B$
- If $HR >> 1$
  - $\bar{\boldsymbol{\sigma}}'_{H_{Failure}}\left(\mathbf{x}_{i_{Failure}}\right) \approx \dot{\boldsymbol{\sigma}}'_T$
  - $\boldsymbol{\sigma}'_{Failure}\left(\mathbf{x}_{i_{Failure}}, t_{Failure}\right) \approx \boldsymbol{\sigma}'_{H_{Failure}}\left(\mathbf{x}_{i_{Failure}}\right)$
  - $\bar{\boldsymbol{\sigma}}'_{Failure}\left(\mathbf{x}_{i_{Failure}}, t_{Failure}\right) \approx \dot{\boldsymbol{\sigma}}'_T$
- As HR increases
  - $\bar{\boldsymbol{\sigma}}'_{H_{Failure}}\left(\mathbf{x}_{i_{Failure}}\right)$ becomes increasingly biased toward $\dot{\boldsymbol{\sigma}}'_T$ instead of $\boldsymbol{\sigma}'_B$
  - $\boldsymbol{\sigma}'_{H_{Failure}}\left(\mathbf{x}_{i_{Failure}}\right)$ becomes increasingly important in the $\boldsymbol{\sigma}'_{Failure}\left(\mathbf{x}_{i_{Failure}}, t_{Failure}\right)$ equation.
  - Therefore, $\bar{\boldsymbol{\sigma}}'_{Failure}\left(\mathbf{x}_{i_{Failure}}, t_{Failure}\right)$ rotates from $\boldsymbol{\sigma}'_B$ to $\dot{\boldsymbol{\sigma}}'_T$.
  - And the heterogeneity of $\boldsymbol{\sigma}'_{Failure}\left(\mathbf{x}_{i_{Failure}}, t_{Failure}\right)$ increases.

Demonstration of the Bias Toward $\dot{\boldsymbol{\sigma}}'_T$ as Heterogeneity Increases: Simulations of the San Gabriel Mountains and the Southern San Andreas Fault Zone

In this section we simulate two different regions, the San Gabriel Mountains, Region #1, and the Southern San Andreas Fault Zones, Region #2, which we assume to have different background stresses, $\boldsymbol{\sigma}'_{B1}$ and $\boldsymbol{\sigma}'_{B2}$ (Figures 4.3 and 4.4). The same stress rate is applied, $\dot{\boldsymbol{\sigma}}'_T$, which is simply oriented $45°$ relative to the major plate boundary, the San Andreas Fault (Figure 4.5, bottom). As spatial heterogeneity increases, the simulations rotate from their respective background orientations ($\boldsymbol{\sigma}'_{B1}$ and $\boldsymbol{\sigma}'_{B2}$) to the stress rate orientation, $\dot{\boldsymbol{\sigma}}'_T$ (Figure 4.5). We run a series of simulations for each region with 32 different heterogeneity ratios, HR, spanning $0.1 \le HR \le 100$ and for $\alpha = 0.0, 0.5, 1.0,$ and 1.5. We save the first 2,000 failures as our synthetic focal mechanisms, $\boldsymbol{\sigma}'_{Failure}\left(\mathbf{x}_{i_{Failure}}, t_{Failure}\right)$. Indeed, as HR increases, $\bar{\boldsymbol{\sigma}}'_{Failure}\left(\mathbf{x}_{i_{Failure}}, t_{Failure}\right)$ rotates from $\boldsymbol{\sigma}'_B$ to $\dot{\boldsymbol{\sigma}}'_T$ and the heterogeneity of $\boldsymbol{\sigma}'_{Failure}\left(\mathbf{x}_{i_{Failure}}, t_{Failure}\right)$ increases as seen in P-T plots of $\boldsymbol{\sigma}'_{Failure}\left(\mathbf{x}_{i_{Failure}}, t_{Failure}\right)$ (Figures 4.6–4.7). Figure 4.8 is interesting because it visually displays that the simulation failures tend to occur at the intersection of $\dfrac{dI'_2(\mathbf{x}_i, t)}{dt} > 0$ and $\dfrac{\frac{2}{3}\tau_0^2 - I'_2(\mathbf{x}_i, 0)}{\frac{2}{3}\tau_0^2} \le 5\%$ (the top 5% of the points close to the failure threshold), per our previous discussion.

One detail we need to emphasize is that since we are using a plastic yield criterion in this chapter, similar to Coulomb Failure with $\mu = 0.0$, failures occurs on maximally

orientated planes, ± 45° from the σ_1 and σ_3 axes. This means that the P axis is aligned with the σ_1 principal stress, and the T axis is aligned with the σ_3 principal stress. Generally, the P and T axes are not aligned with the principal stresses, as in the case of Coulomb Failure with $\mu > 0.0$. Appendix A explains the mathematics behind this. For this chapter, however, we use the special case of maximally oriented planes, which have P and T axes aligned with σ_1 and σ_3 respectively.

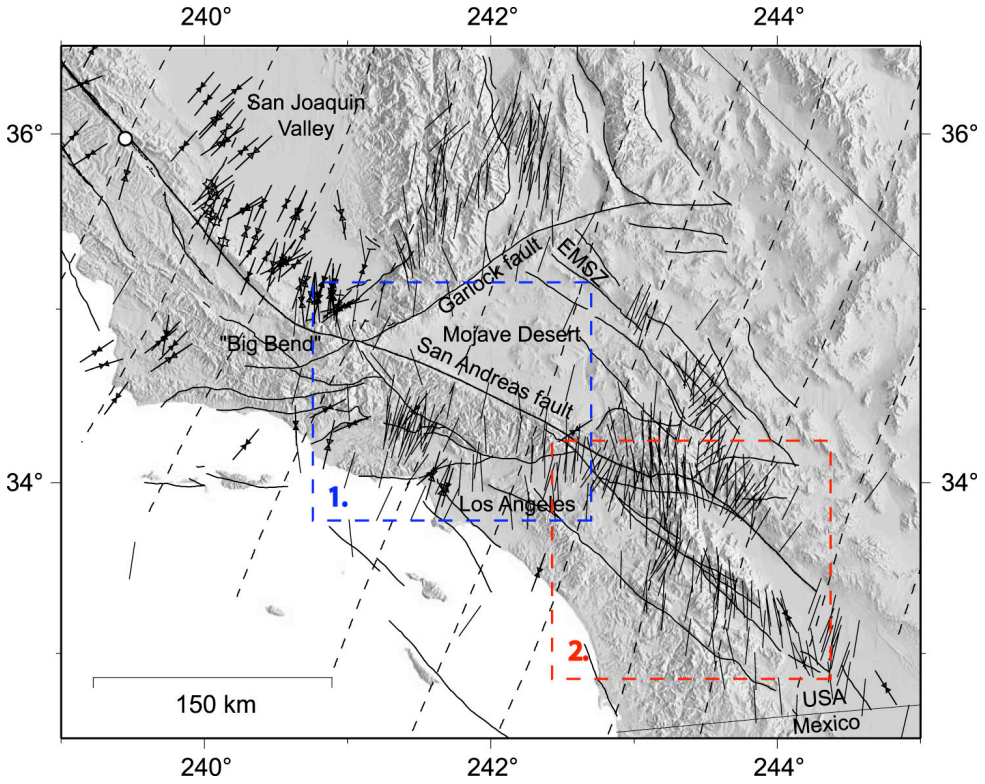

Figure 4.3. *Figure modified from Townend and Zoback [2004]. The dashed box with the #1 is magnified in Figure 4.4 a) to zoom in on the San Gabriel Mountains, our Region #1. The dashed red box with the #2 is magnified in Figure 4.4 b) to zoom in on the Southern San Andreas Fault, our Region #2. The orientations of maximum compressive stress in the Townend and Zoback figure are calculated using earthquake focal mechanism inversions, borehole breakouts, and hydraulic fracturing.*

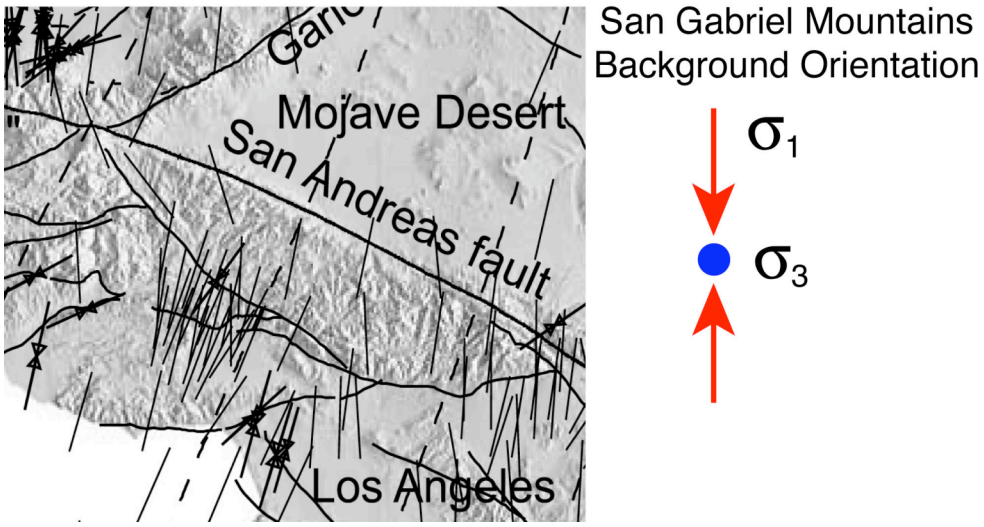

a)

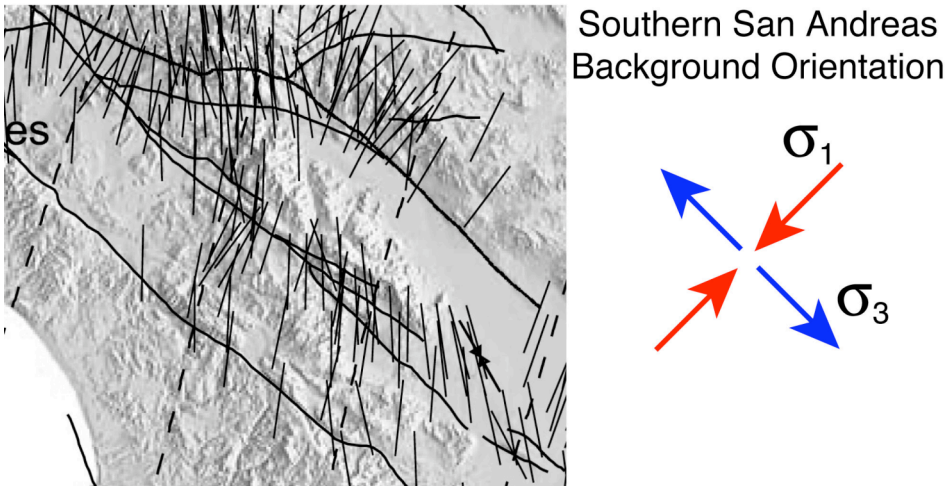

b)

Figure 4.4. *a) is a magnified inset from Figure 4.3. The diagram to the right shows the stress orientation we use for the San Gabriel Mountains background stress,* $\boldsymbol{\sigma}'_{B1}$. *We also have drawn the* σ_1 *and* σ_3 *axes next to the inset, where the inward pointing, red arrows indicate a* $N-S$ *direction of the principal compression axis, and the small blue circle indicates a vertical direction of the principal tension axis. In b) we have the second magnified inset from Figure 4.3. The diagram to the right shows the stress orientation used for our Southern San Andreas simulations background stress,* $\boldsymbol{\sigma}'_{B2}$, *with a principal compressive stress direction (red arrows) almost perpendicular to the fault.*

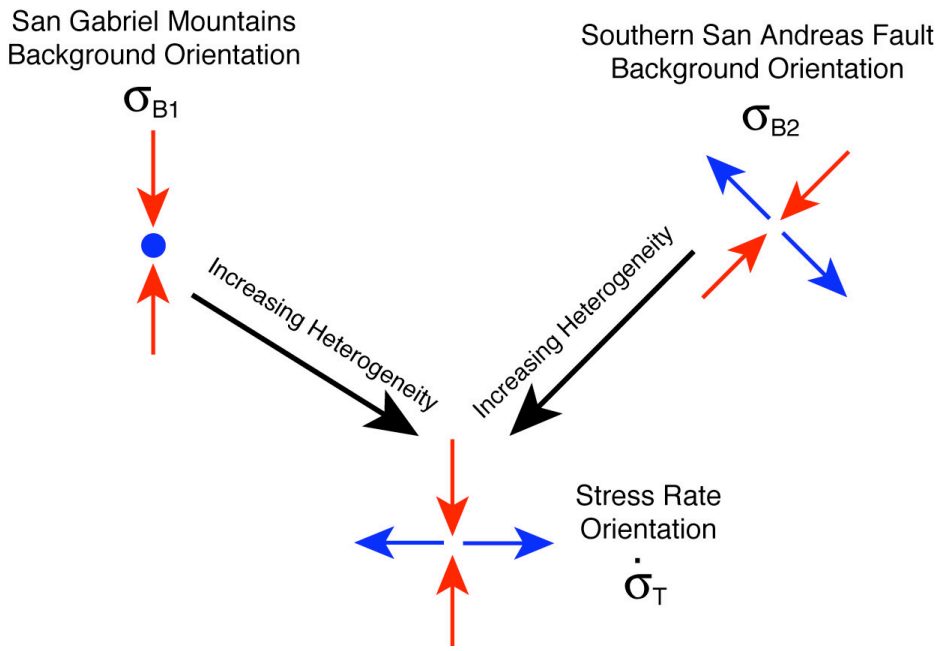

Figure 4.5. *The inward pointing red arrows for* $\boldsymbol{\sigma}_{B1}$, $\boldsymbol{\sigma}_{B2}$, *and* $\dot{\boldsymbol{\sigma}}_T$ *show the directions of their respective* σ_1 *axes. The outward pointing blue arrows for* $\boldsymbol{\sigma}_{B2}$ *and* $\dot{\boldsymbol{\sigma}}_T$ *and the upward/downward blue arrow represented by the blue circle for* $\boldsymbol{\sigma}_{B1}$ *show the directions of their respective* σ_3 *axes. As the amplitude of spatial heterogeneity,* HR, *increases, the simulation stress tensors (component-wise average of the first 2,000 points that fail in our 3D grid) increasingly rotate from the background stress to the stress rate,* $\dot{\boldsymbol{\sigma}}'_T$. *Even though our two regions, the San Gabriel Mountains and the Southern San Andreas Fault, have very different background stresses, as* HR *increases, the simulations for the two regions will become increasing similar until for* $HR \gg 1$ *they will be indistinguishable from one another and will have an average failure stress tensor,* $\bar{\boldsymbol{\sigma}}'_{Failure}\left(\mathbf{x}_{i_{Failure}}, t_{Failure}\right)$, *aligned with stress rate,* $\dot{\boldsymbol{\sigma}}'_T$. *Figures 4.6–4.7 demonstrate this effect with P-T plots of simulations for different values of* HR.

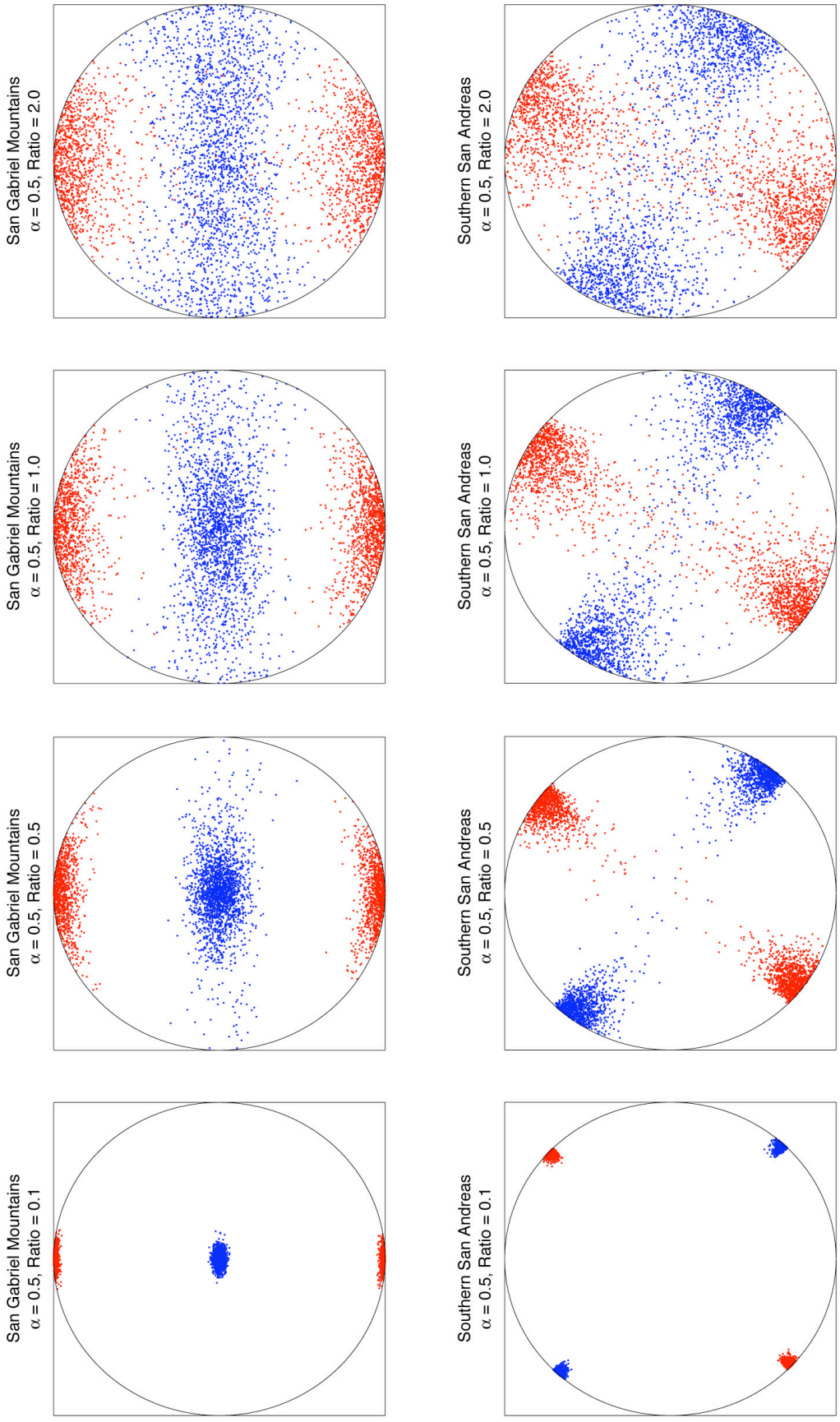
San Gabriel Mountains
α = 0.5, Ratio = 2.0
Southern San Andreas
α = 0.5, Ratio = 2.0
San Gabriel Mountains
α = 0.5, Ratio = 1.0
Southern San Andreas
α = 0.5, Ratio = 1.0
San Gabriel Mountains
α = 0.5, Ratio = 0.5
Southern San Andreas
α = 0.5, Ratio = 0.5
San Gabriel Mountains
α = 0.5, Ratio = 0.1
Southern San Andreas
α = 0.5, Ratio = 0.1

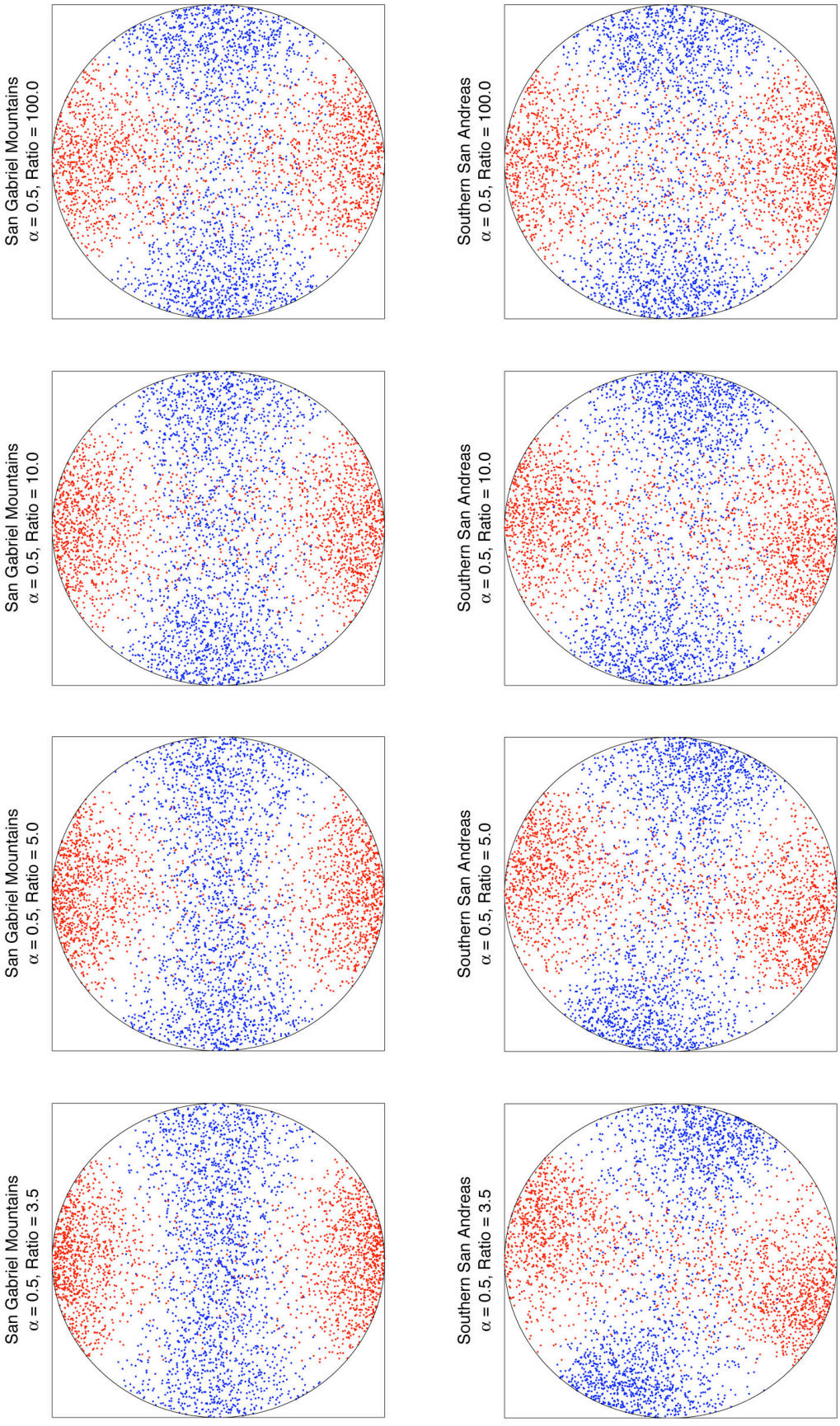
San Gabriel Mountains
α = 0.5, Ratio = 100.0
Southern San Andreas
α = 0.5, Ratio = 100.0
San Gabriel Mountains
α = 0.5, Ratio = 10.0
Southern San Andreas
α = 0.5, Ratio = 10.0
San Gabriel Mountains
α = 0.5, Ratio = 5.0
Southern San Andreas
α = 0.5, Ratio = 5.0
San Gabriel Mountains
α = 0.5, Ratio = 3.5
Southern San Andreas
α = 0.5, Ratio = 3.5

Figure 4.6. *P-T plots of Region #1 on top, the San Gabriel Mountains, and Region #2 on the bottom, the Southern San Andreas, for different levels of spatial heterogeneity,* $HR = \frac{\sqrt{Mean\left[\ \boldsymbol{\sigma}'_H(\mathbf{x}_i) : \boldsymbol{\sigma}'_H(\mathbf{x}_i)\right]}}{\sqrt{\boldsymbol{\sigma}'_B : \boldsymbol{\sigma}'_B}}$. *The spatial smoothing* α *shown here is* $\alpha = 0.5$, *and the plots for* $\alpha = 0.0$ *and* $\alpha = 1.0$ *look almost identical. The P axes are in red and the T axes are in blue.* HR, *which compares the relative size of the heterogeneous stress to the background stress, increases from* $HR = 0.1$ *(almost no heterogeneity) to* $HR = 100$ *(almost all heterogeneity). For* $HR = 0.1$, *there is little to no scatter of the P-T orientations, and they are centered on the respective background stress orientations,* $\boldsymbol{\sigma}'_{B1}$ *and* $\boldsymbol{\sigma}'_{B2}$. *As* HR *increases, the scatter of the P-T axes increases, and the average orientations of the simulations rotate toward the stress rate orientation,* $\dot{\boldsymbol{\sigma}}'_T$. *It becomes increasingly difficult to distinguish between the two regions as the spatial stress heterogeneity increases, until for* $HR = 100$, *the San Gabriel Mountains simulations and the Southern San Andreas Fault simulations look almost identical. If stress heterogeneity in the real Earth is this extreme, one could only measure the stress rate,* $\dot{\boldsymbol{\sigma}}'_T$; *there would be no information for determining the actual background stress, which could be quite different from* $\dot{\boldsymbol{\sigma}}'_T$.

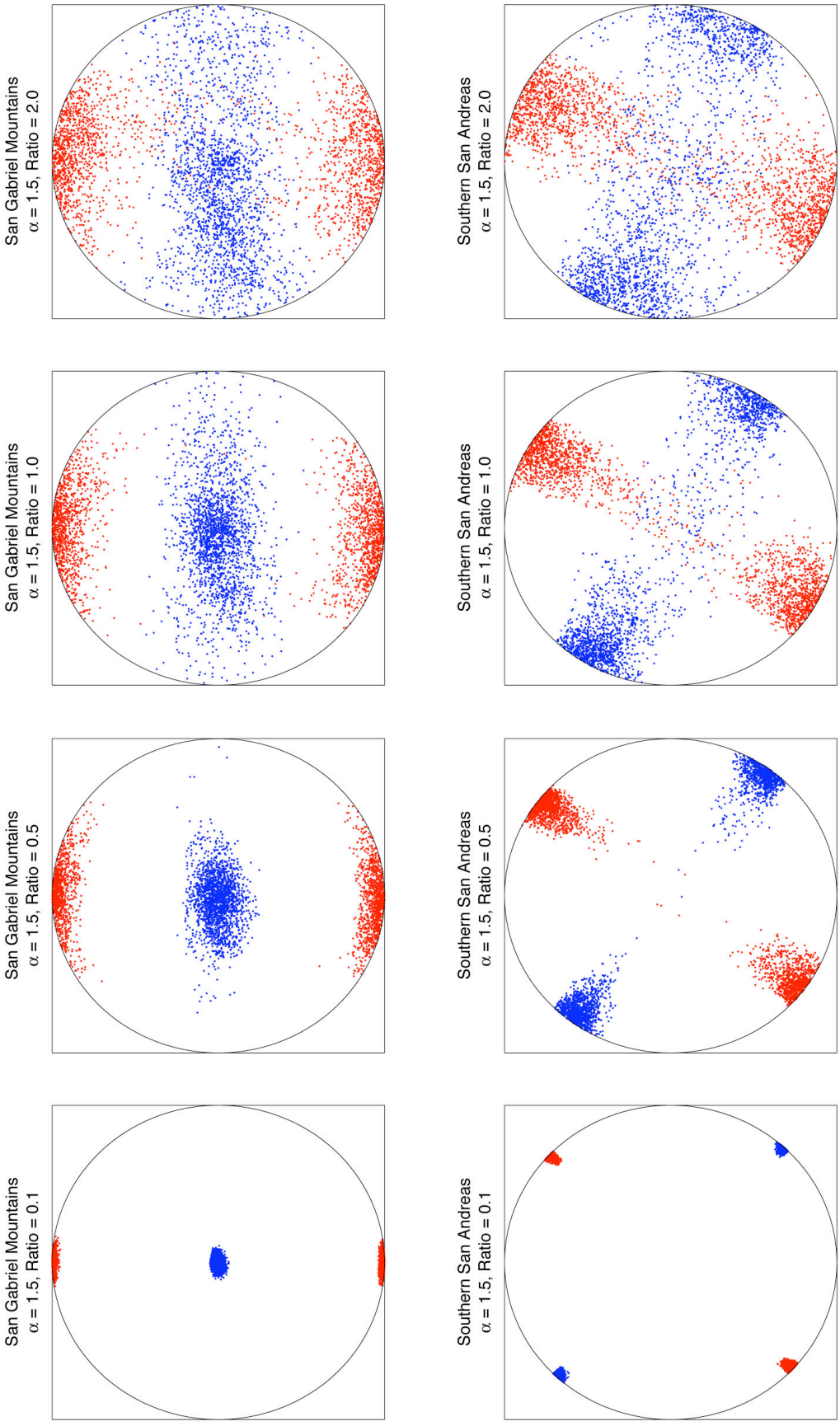
San Gabriel Mountains
α = 1.5, Ratio = 2.0
Southern San Andreas
α = 1.5, Ratio = 2.0
San Gabriel Mountains
α = 1.5, Ratio = 1.0
Southern San Andreas
α = 1.5, Ratio = 1.0
San Gabriel Mountains
α = 1.5, Ratio = 0.5
Southern San Andreas
α = 1.5, Ratio = 0.5
San Gabriel Mountains
α = 1.5, Ratio = 0.1
Southern San Andreas
α = 1.5, Ratio = 0.1

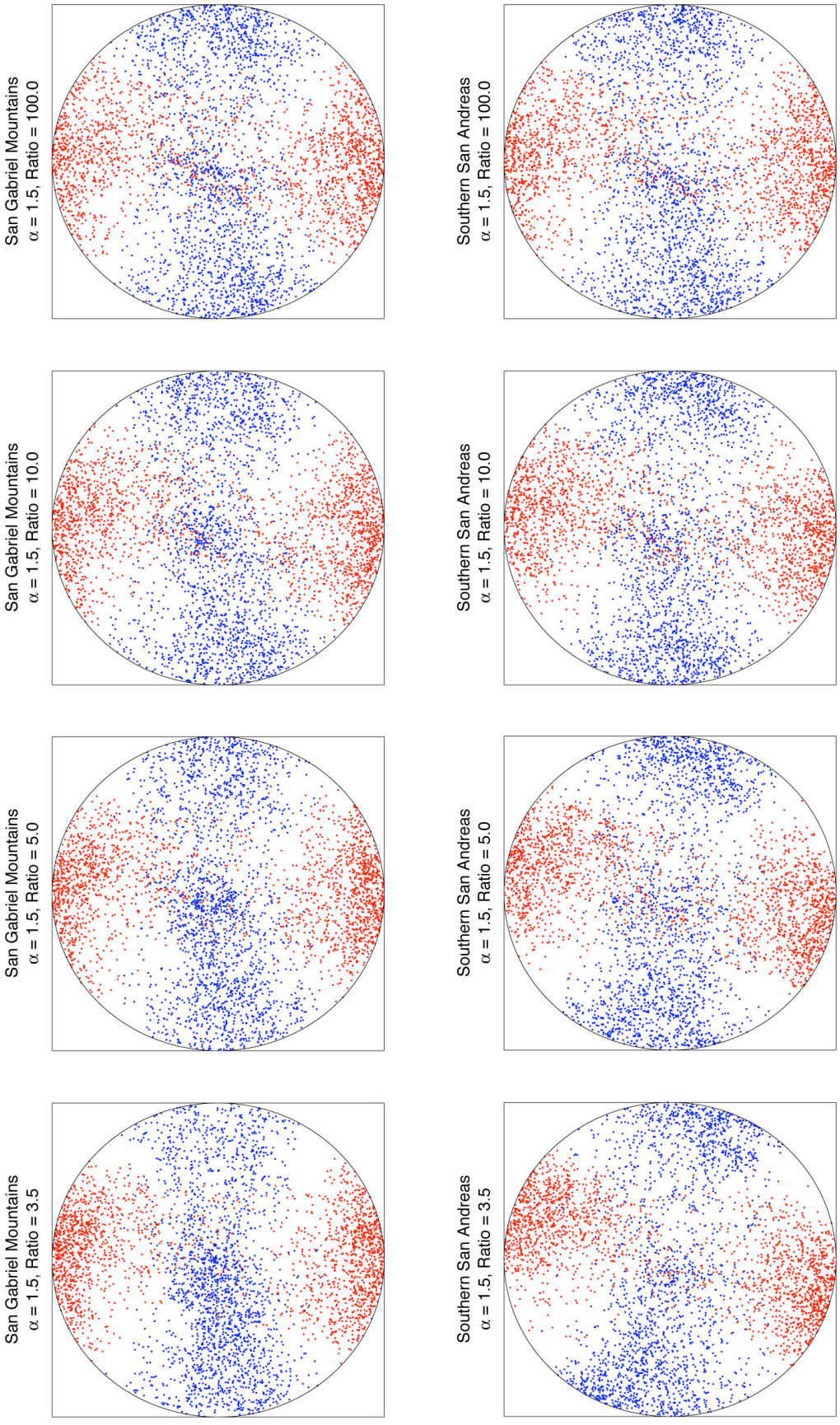
San Gabriel Mountains
α = 1.5, Ratio = 100.0
Southern San Andreas
α = 1.5, Ratio = 100.0
San Gabriel Mountains
α = 1.5, Ratio = 10.0
Southern San Andreas
α = 1.5, Ratio = 10.0
San Gabriel Mountains
α = 1.5, Ratio = 5.0
Southern San Andreas
α = 1.5, Ratio = 5.0
San Gabriel Mountains
α = 1.5, Ratio = 3.5
Southern San Andreas
α = 1.5, Ratio = 3.5

Figure 4.7. *P-T plots of Region #1 on top, the San Gabriel Mountains, and Region #2 on the bottom, the Southern San Andreas, for different levels of spatial heterogeneity,* $HR = \frac{\sqrt{Mean\left[\ \boldsymbol{\sigma}'_H(\mathbf{x}_i) : \boldsymbol{\sigma}'_H(\mathbf{x}_i)\right]}}{\sqrt{\boldsymbol{\sigma}'_B : \boldsymbol{\sigma}'_B}}$. *The spatial smoothing* α *shown here is* $\alpha = 1.5$, *and the effect of the spatial smoothing is apparent in the P-T plots. The same heterogeneous grid is used for all the simulations with* $\alpha = 1.5$ *and one can see how the spatial filtering distorts the P-T patterns seen in the simulations for* $\alpha \le 1.0$. *There is still a rotation as* HR *increases as seen in Figure 4.6 and for* $HR = 100$, *the two regions become indistinguishable as in Figure 4.6. This degree of spatial smoothing is unrealistic for the real Earth but is kept as an end-member case.*

σ_H for $l'_2(x_i,0)$ Near Failure, t_0 at 95%
P Axes for α = 0.0, Ratio = 1.0

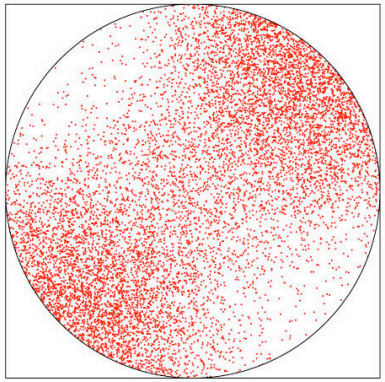

σ_H for $l'_2(x_i,0)$ Near Failure, t_0 at 95%
T Axes for α = 0.0, Ratio = 1.0

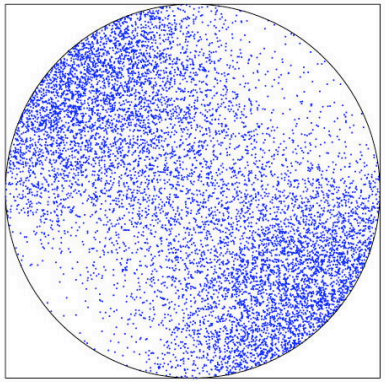

Comparison Plot, σ_H
P Axes for α = 0.0, Ratio = 1.0

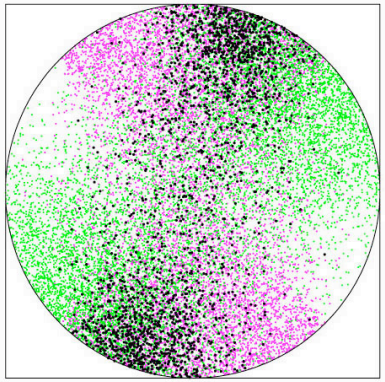

Comparison Plot, σ_H
T Axes for α = 0.0, Ratio = 1.0

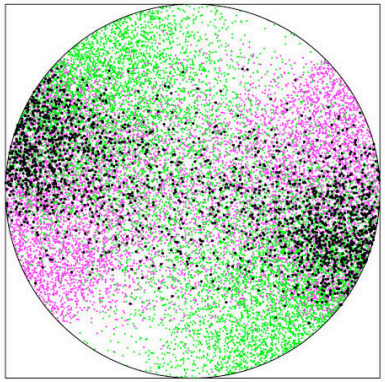

Random σ_H for $dl'_2/dt > 0$
P Axes for α = 0.0, Ratio = 1.0

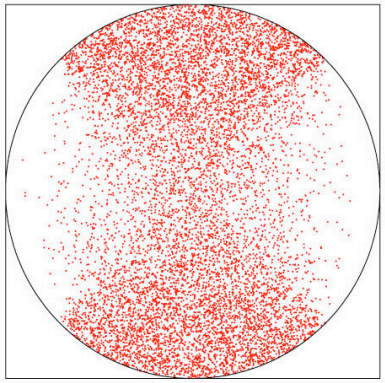

Random σ_H for $dl'_2/dt > 0$
T Axes for α = 0.0, Ratio = 1.0

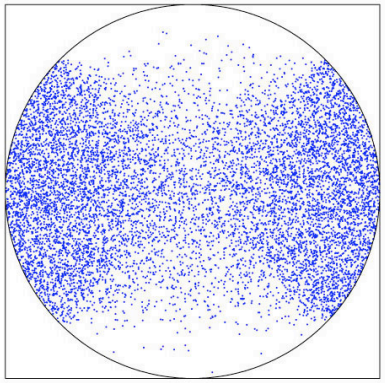

First 2,000 Failures, σ_H
P Axes for α = 0.0, Ratio = 1.0

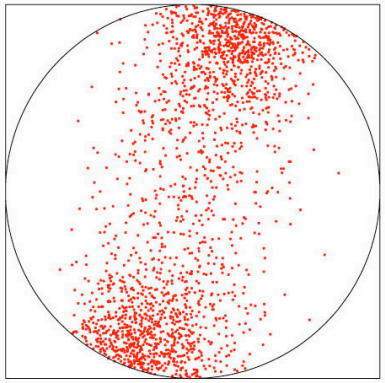

First 2,000 Failures, σ_H
T Axes for α = 0.0, Ratio = 1.0

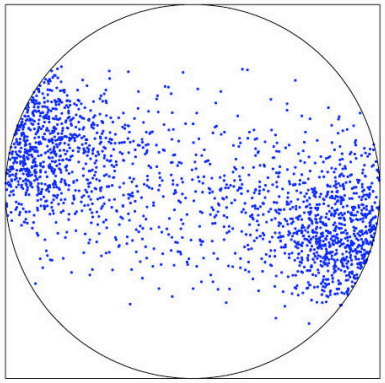

Figure 4.8. *This figure containing P-T plots is taken from the simulation for Region #2, the Southern San Andreas Fault, with* $\alpha = 0.0$, *and* $HR = 1.0$. *It is intended to show that simulation failures tend to occur at the intersection of* $\frac{dI_2'(\mathbf{x}_i,t)}{dt} > 0$ *and* $\frac{\frac{2}{3}\tau_0^2 - I_2'(\mathbf{x}_i,0)}{\frac{2}{3}\tau_0^2} \le 5\%$ *(the top* 5% *of the points close to the failure threshold). All the plots in this figure show the orientations of* $\boldsymbol{\sigma}_H'(\mathbf{x}_i)$, *not the full stress tensor. The top left two plots are the P axes in red and the T axes in blue for the points close to the failure threshold,* $\frac{2}{3}\tau_0^2$; *i.e., the 10,000 points plotted are a random sampling of those points within the 3D heterogeneous grid where* $\frac{\frac{2}{3}\tau_0^2 - I_2'(\mathbf{x}_i,0)}{\frac{2}{3}\tau_0^2} \le 5\%$ *is true. The bottom left two plots are the P axes and T axes for points going toward failure; i.e., the 10,000 points plotted are a random sampling of those points where* $\frac{dI_2'(\mathbf{x}_i,t)}{dt} > 0$ *is true. The bottom right two plots show the P and T axes for the first 2,000 failures within the simulation. The top right two plots compare all three quantities and show that the simulation failures do indeed occur at the intersection of* $\frac{dI_2'(\mathbf{x}_i,t)}{dt} > 0$ *and* $\frac{\frac{2}{3}\tau_0^2 - I_2'(\mathbf{x}_i,0)}{\frac{2}{3}\tau_0^2} \le 5\%$. $\frac{\frac{2}{3}\tau_0^2 - I_2'(\mathbf{x}_i,0)}{\frac{2}{3}\tau_0^2} \le 5\%$ *is plotted in green,* $\frac{dI_2'(\mathbf{x}_i,t)}{dt} > 0$ *is plotted in magenta, and the first 2,000 simulation failures are plotted in black. Note that the black points occur at the intersection of the green and magenta.*

Quantifying the Rotation from $\boldsymbol{\sigma}'_B$ to $\dot{\boldsymbol{\sigma}}'_T$ as Heterogeneity Increases

The most obvious way to quantify the rotation from $\boldsymbol{\sigma}'_B$ to $\dot{\boldsymbol{\sigma}}'_T$ as heterogeneity increases, HR increasing, would be to calculate the following: 1) The angular difference between $\bar{\boldsymbol{\sigma}}'_{Failure}\left(\mathbf{x}_{i_{Failure}}, t_{Failure}\right)$ and $\boldsymbol{\sigma}'_B$, which we call $\angle\bar{\boldsymbol{\sigma}}'_{Failure}\boldsymbol{\sigma}'_B$. 2) The angular difference between $\bar{\boldsymbol{\sigma}}'_{Failure}\left(\mathbf{x}_{i_{Failure}}, t_{Failure}\right)$ and $\dot{\boldsymbol{\sigma}}'_T$, which we call $\angle\bar{\boldsymbol{\sigma}}'_{Failure}\dot{\boldsymbol{\sigma}}'_T$. As HR increases and the average failure orientations rotate from $\boldsymbol{\sigma}'_B$ to $\dot{\boldsymbol{\sigma}}'_T$, $\angle\bar{\boldsymbol{\sigma}}'_{Failure}\boldsymbol{\sigma}'_B$ will increase and $\angle\bar{\boldsymbol{\sigma}}'_{Failure}\dot{\boldsymbol{\sigma}}'_T$ will decrease. If we wish to normalize this quantity, we can calculate $\frac{\angle\bar{\boldsymbol{\sigma}}'_{Failure}\boldsymbol{\sigma}'_B}{\angle\boldsymbol{\sigma}'_B\dot{\boldsymbol{\sigma}}'_T}$ and $\frac{\angle\bar{\boldsymbol{\sigma}}'_{Failure}\dot{\boldsymbol{\sigma}}'_T}{\angle\boldsymbol{\sigma}'_B\dot{\boldsymbol{\sigma}}'_T}$, which typically have values ranging from ≈ 0.0 to ≈ 1.0. For example, if $\frac{\angle\bar{\boldsymbol{\sigma}}'_{Failure}\boldsymbol{\sigma}'_B}{\angle\boldsymbol{\sigma}'_B\dot{\boldsymbol{\sigma}}'_T} = 0.0$, the points that have failed in the simulation are on average aligned with the background stress, $\boldsymbol{\sigma}'_B$. This is what we would expect for $HR = 0.0$. Concurrently, we would expect $\frac{\angle\bar{\boldsymbol{\sigma}}'_{Failure}\dot{\boldsymbol{\sigma}}'_T}{\angle\boldsymbol{\sigma}'_B\dot{\boldsymbol{\sigma}}'_T} \approx 1.0$ if $\frac{\angle\bar{\boldsymbol{\sigma}}'_{Failure}\boldsymbol{\sigma}'_B}{\angle\boldsymbol{\sigma}'_B\dot{\boldsymbol{\sigma}}'_T} = 0.0$. If $HR \to \infty$, then we would expect the reverse, $\frac{\angle\bar{\boldsymbol{\sigma}}'_{Failure}\dot{\boldsymbol{\sigma}}'_T}{\angle\boldsymbol{\sigma}'_B\dot{\boldsymbol{\sigma}}'_T} \approx 0.0$ and $\frac{\angle\bar{\boldsymbol{\sigma}}'_{Failure}\boldsymbol{\sigma}'_B}{\angle\boldsymbol{\sigma}'_B\dot{\boldsymbol{\sigma}}'_T} \approx 1.0$, where the points that have failed in the simulation are on average aligned with $\dot{\boldsymbol{\sigma}}'_T$.

If $\frac{\angle\bar{\boldsymbol{\sigma}}'_{Failure}\boldsymbol{\sigma}'_B}{\angle\boldsymbol{\sigma}'_B\dot{\boldsymbol{\sigma}}'_T} \approx \angle\boldsymbol{\sigma}'_B\dot{\boldsymbol{\sigma}}'_T - \frac{\angle\bar{\boldsymbol{\sigma}}'_{Failure}\dot{\boldsymbol{\sigma}}'_T}{\angle\boldsymbol{\sigma}'_B\dot{\boldsymbol{\sigma}}'_T}$, then we know that the angular difference is purely due to a tradeoff of $\boldsymbol{\sigma}'_B$ and $\dot{\boldsymbol{\sigma}}'_T$, not any other orientations (except for small fluctuations due to randomness in the grid); consequently, we can think of these as: 1) normalized angular differences in terms of the normalized bias toward the stressing rate tensor, $\dot{\boldsymbol{\sigma}}'_T$, where

$\frac{\angle\bar{\boldsymbol{\sigma}}'_{Failure}\boldsymbol{\sigma}'_B}{\angle\boldsymbol{\sigma}'_B\dot{\boldsymbol{\sigma}}'_T} \approx \angle\boldsymbol{\sigma}'_B\dot{\boldsymbol{\sigma}}'_T - \frac{\angle\bar{\boldsymbol{\sigma}}'_{Failure}\dot{\boldsymbol{\sigma}}'_T}{\angle\boldsymbol{\sigma}'_B\dot{\boldsymbol{\sigma}}'_T} \approx Normalized\ Bias$ (% rotation toward $\dot{\boldsymbol{\sigma}}'_T$) and 2) angular differences in terms of the angular bias toward the stressing rate tensor, where $\angle\bar{\boldsymbol{\sigma}}'_{Failure}\boldsymbol{\sigma}'_B \approx \angle\boldsymbol{\sigma}'_B\dot{\boldsymbol{\sigma}}'_T - \angle\bar{\boldsymbol{\sigma}}'_{Failure}\dot{\boldsymbol{\sigma}}'_T \approx Bias$ (angular rotation toward $\dot{\boldsymbol{\sigma}}'_T$).

The next question we have to address in quantifying the relationship between the stress heterogeneity, HR, and $Bias$ / $Normalized\ Bias$, is how to calculate the angular difference between our average failure stress tensor, $\bar{\boldsymbol{\sigma}}'_{Failure}\left(\mathbf{x}_{i_{Failure}}, t_{Failure}\right)$, and either $\boldsymbol{\sigma}'_B$ or $\dot{\boldsymbol{\sigma}}'_T$. In the real Earth, we have limitations on the information we can glean about the stress field using earthquakes. For a single focal mechanism, we can determine only the orientations of the P, T, and B axes (three-parameters). If one assumes the Hencky-Mises failure criterion and maximally oriented planes then this also gives us the orientation of the three principal stresses (three-parameters); however, if we invert a set of focal mechanisms, we can determine both the orientations of the three principal stresses (without having to assume maximally oriented planes) and the stress ratio, $R = \left(\frac{\sigma_2 - \sigma_3}{\sigma_1 - \sigma_3}\right)$ [e.g., *Rivera and Kanamori*, 2002] (four-parameters). This means that a focal mechanism inversion can yield the relative sizes of the components within the failure deviatoric stress tensor, but not the overall size.

This leads us to two different methodologies for quantifying the angular difference between two stress tensors. The first methodology calculates the minimum angular difference when only the three orientation parameters are available. This is particularly helpful when comparing individual focal mechanism orientations. One would determine the four different possible sets of strike, dip, and rake, $(\Theta, \delta, \lambda)$, for

each focal mechanism or stress tensor, allowing for $0 \le \delta \le 180°$ (Appendix A). Then one would convert the four sets of $(\Theta, \delta, \lambda)$ into quaternions for each focal mechanism or stress tensor. Last, using quaternion algebra (see Chapter 3), one would calculate the minimum rotation between two focal mechanisms or stress tensors, by calculating the 16 possible sets of $(\omega_R, [\theta_R, \phi_R])$ and choose the minimum ω_R.

The second methodology uses the scalar product of two deviatoric stress tensors to calculate an angular difference. Since the scalar product is a scalar quantity, invariant upon rotation, we can define an angle between the rank two tensors, A and B, as

$$\angle AB = \cos^{-1}\left(\frac{A:B}{\|A\|\|B\|}\right) \tag{4.25}$$

where

$$\|A\| = \sqrt{A:A}$$

and

$$\|B\| = \sqrt{B:B}.$$

Note that this measure of angular difference yields a result different from ω_R. It isn't a physical rotation in 3D space. Instead, it is a measure of the similarity of the two tensors including information about the relative sizes of the eigenvalues.

Since a deviatoric stress tensor has five independent quantities, normalizing by $\|A\|\|B\|$ reduces the independent quantities to four in the calculation of $\angle AB$; therefore, this type of calculation of angular difference is most useful when we know both the orientations of the three principal stresses and one other quantity like the stress ratio as in

focal mechanism inversions. From the three principal stresses and stress ratio, one way to reconstruct the deviatoric stress tensor would be as follows:

- Let $\sigma_3' = 1.0$
- Combine the stress ratio equation, $R = \left(\frac{\sigma_2' - \sigma_3'}{\sigma_1' - \sigma_3'} \right)$, and the deviatoric constraint $\sigma_1' + \sigma_2' + \sigma_3' = 0$ to derive $\sigma_1' = -\left(\frac{2 - R}{1 + R} \right) \sigma_3'$.
- Then let, $\sigma_2' = -\left(\sigma_1' + \sigma_3' \right)$
- Then combine these principal stresses with principal orientations to produce the deviatoric stress tensor. See Appendix A.

As expected, the overall size of this deviatoric stress tensor is unspecified, but it does yield the relative sizes of each component.

In Figures 4.9–4.12, we apply these two different methodologies for calculating the angular difference between $\bar{\boldsymbol{\sigma}}'_{Failure}\left(\mathbf{x}_{i_{Failure}}, t_{Failure} \right)$ and $\boldsymbol{\sigma}'_B$ for our two regions, San Gabriel Mountains and the Southern San Andreas Fault. Figures 4.9 and 4.10 plot the rotation away from $\boldsymbol{\sigma}'_B$ toward $\dot{\boldsymbol{\sigma}}'_T$ as a function of heterogeneity for our two regions using our first methodology, by showing the three-parameter *Bias* in Figure 4.9 and the three-parameter *Normalized Bias* in Figure 4.10. Figures 4.11 and 4.12 plot the same quantities as 4.9 and 4.10; only this time, we use the second methodology, four-parameter *Bias* in Figure 4.11 and four parameter *Normalized Bias* in Figure 4.12. Each point on the plots is an average over three simulations with different spatial smoothness, $\alpha = 0.0$, $\alpha = 0.5$, and $\alpha = 1.0$.

Interestingly, when we use the three-parameter method of calculating *Bias* Region #2, the Southern San Andreas, rotates smoothly from the $\boldsymbol{\sigma}'_B$ orientation to the $\dot{\boldsymbol{\sigma}}'_T$ orientation as heterogeneity, HR, increases, but Region #1, the San Gabriel Mountains, does not. Region #1, plotted in blue, quickly jumps from the $\boldsymbol{\sigma}'_B$ orientation to the $\dot{\boldsymbol{\sigma}}'_T$ orientation at $HR \approx 2.0$ (Figures 4.9 and 4.10). When we use the four parameter method of calculating *Bias*, both Region #1 and Region #2 rotate smoothly from $\boldsymbol{\sigma}'_B$ to $\dot{\boldsymbol{\sigma}}'_T$ as heterogeneity, HR, increases (Figures 4.11 and 4.12). This occurs because the stress ratio $R \approx 1.0$ for all HR in Region #2, so it does not really matter which methodology we use, the three-parameter or four-parameter method of calculating angular difference, because all the information is contained in the three principal stress orientations. However, for Region #1, the stress ratio, R, is significantly changing along with the principal stress orientations, and it follows that the three-parameter method of calculating *Bias* is insufficient to fully represent the change in orientation as a function of HR. That is why we see a step function at $HR \approx 2.0$ for Region #1. Regions #1 and #2 are extreme examples of this effect; most combinations of $\boldsymbol{\sigma}'_B$ and $\dot{\boldsymbol{\sigma}}'_T$ will have behavior in between these two for the three-parameter methodology of calculating *Bias*.

At the same time, whenever possible, it is best to use the four-parameter methodology of calculating *Bias*, which uses the inner product to produce stable *Bias* and *Normalized Bias* curves as a function of HR. For example, even though Regions #1 and #2 have very different background stresses, their *Normalized Bias* curves are quite similar. Chapter 5 will expand upon this topic by generating synthetic *Bias* and *Normalized Bias* curves using the four-parameter methodology that can be compared to real data to estimate stress parameters in the real Earth.

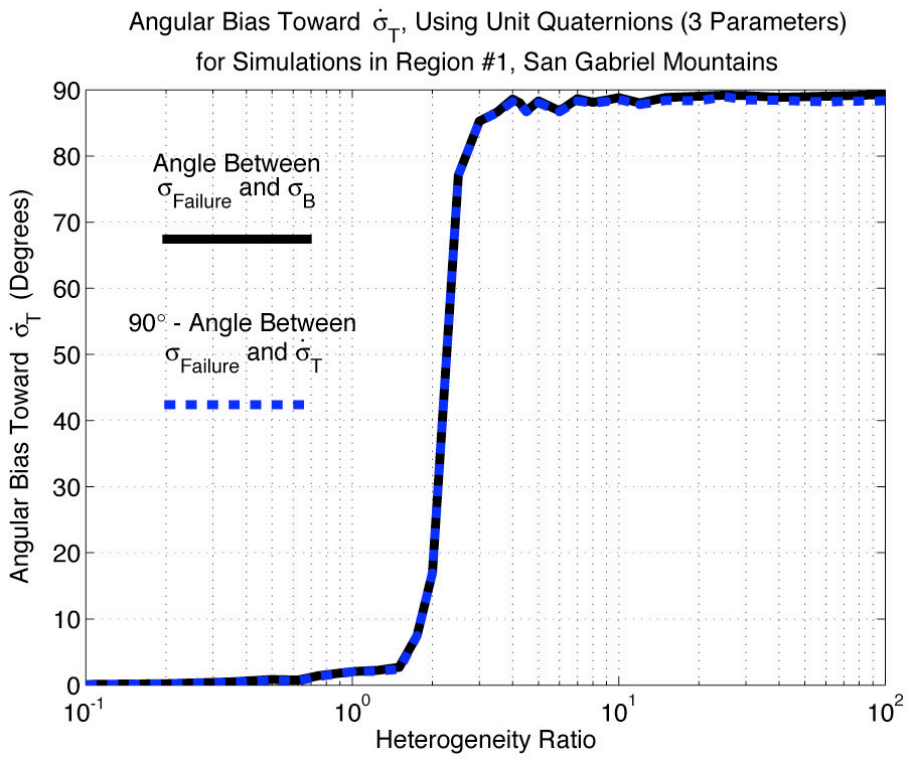

Figure 4.9 a)

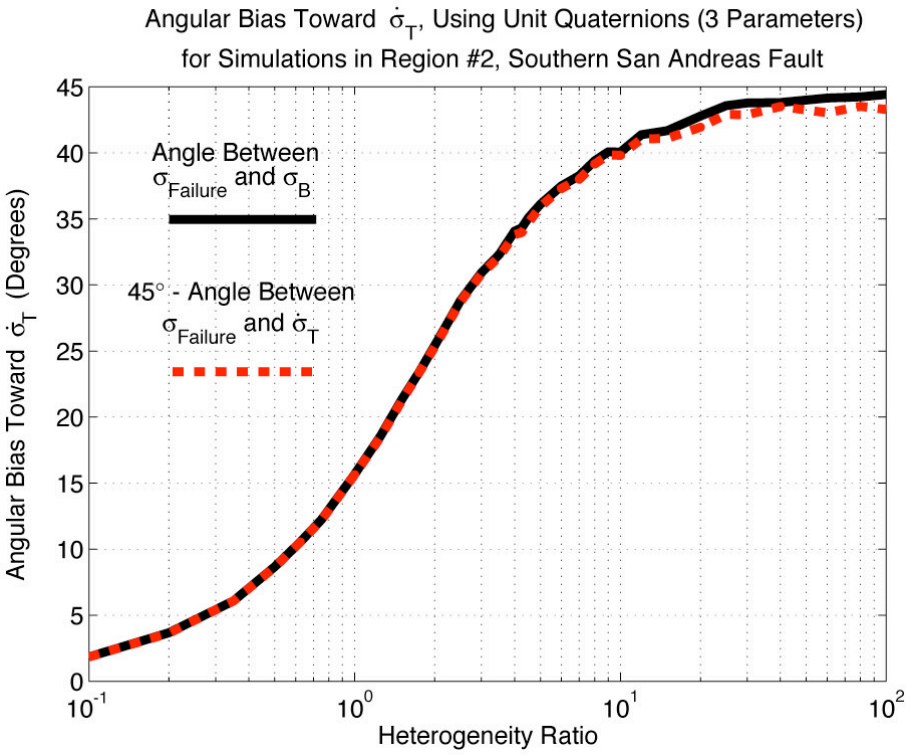

Figure 4.9 b)

Figure 4.9. *Plots of angular Bias toward the stressing rate orientation,* $\dot{\boldsymbol{\sigma}}'_T$*, as a function of heterogeneity ratio,* HR*, for the* ***a)*** *San Gabriel Mountains and the* ***b)*** *Southern San Andreas Fault. Bias is calculated two different ways in this plot. The solid black line shows the angular difference between,* $\bar{\boldsymbol{\sigma}}'_{Failure}\left(\mathbf{x}_{i_{Failure}}, t_{Failure}\right)$ *and* $\boldsymbol{\sigma}'_B$*,* $\angle\bar{\boldsymbol{\sigma}}'_{Failure}\boldsymbol{\sigma}'_B$*, and the dashed red line, which plots almost exactly on top shows* $\angle\boldsymbol{\sigma}'_B\dot{\boldsymbol{\sigma}}'_T - \angle\bar{\boldsymbol{\sigma}}'_{Failure}\dot{\boldsymbol{\sigma}}'$*. The angular difference for these two quantities,* $\angle\bar{\boldsymbol{\sigma}}'_{Failure}\boldsymbol{\sigma}'_B$ *and* $\angle\boldsymbol{\sigma}'_B\dot{\boldsymbol{\sigma}}'_T - \angle\bar{\boldsymbol{\sigma}}'_{Failure}\dot{\boldsymbol{\sigma}}'$*, is calculated using our three-parameter method. This methodology uses quaternions to determine the minimum rotation angle,* ω*, between two focal mechanisms or the principal orientations in a stress tensor. The red dashed line and the solid black lines are averages over simulations with three different levels of spatial smoothing,* $\alpha = 0.0$*,* $\alpha = 0.5$*, and* $\alpha = 1.0$*. The Southern San Andreas simulations smoothly rotate from the* $\boldsymbol{\sigma}'_B$ *orientation to the* $\dot{\boldsymbol{\sigma}}'_T$ *as* HR *increases, but the San Gabriel Mountain simulations jump abruptly from* $\boldsymbol{\sigma}'_B$ *to* $\dot{\boldsymbol{\sigma}}'_T$ *at* $HR \approx 2.0$*. This occurs because our fracture criterion is applied to the deviatoric stress tensor, not just the three orientation angles; hence, one must take into account the changes in the stress ratio,* R*, in addition to changes in the three principal orientations to adequately parameterize the rotation of* $\bar{\boldsymbol{\sigma}}'_{Failure}\left(\mathbf{x}_{i_{Failure}}, t_{Failure}\right)$ *from* $\boldsymbol{\sigma}'_B$ *to* $\dot{\boldsymbol{\sigma}}'_T$ *as* HR *increases for any pair of* $\boldsymbol{\sigma}'_B$ *and* $\dot{\boldsymbol{\sigma}}'_T$*.*

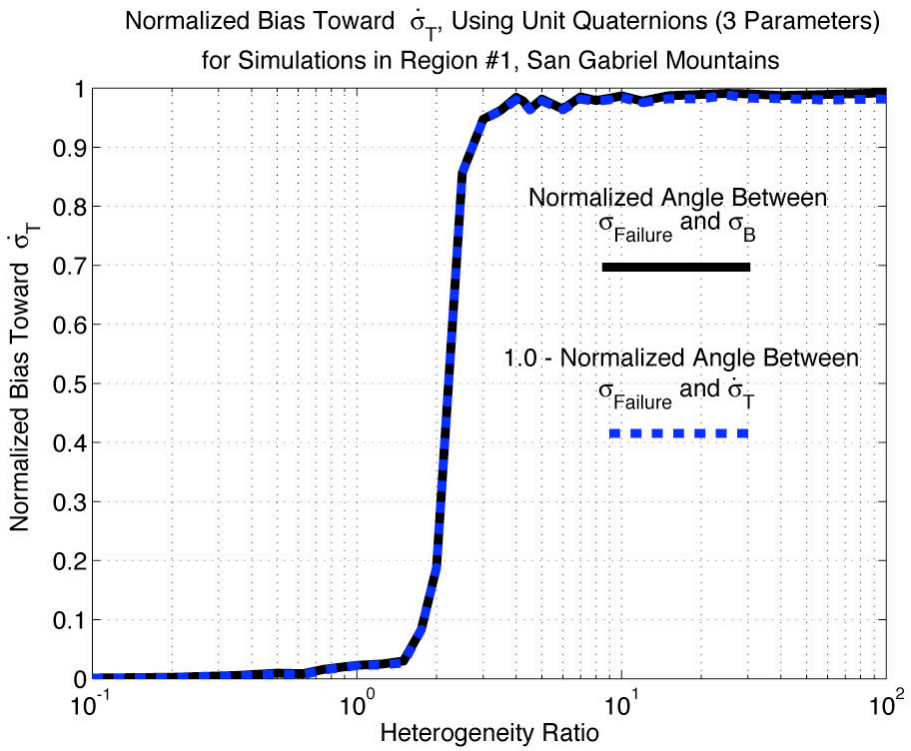

Figure 4.10 a)

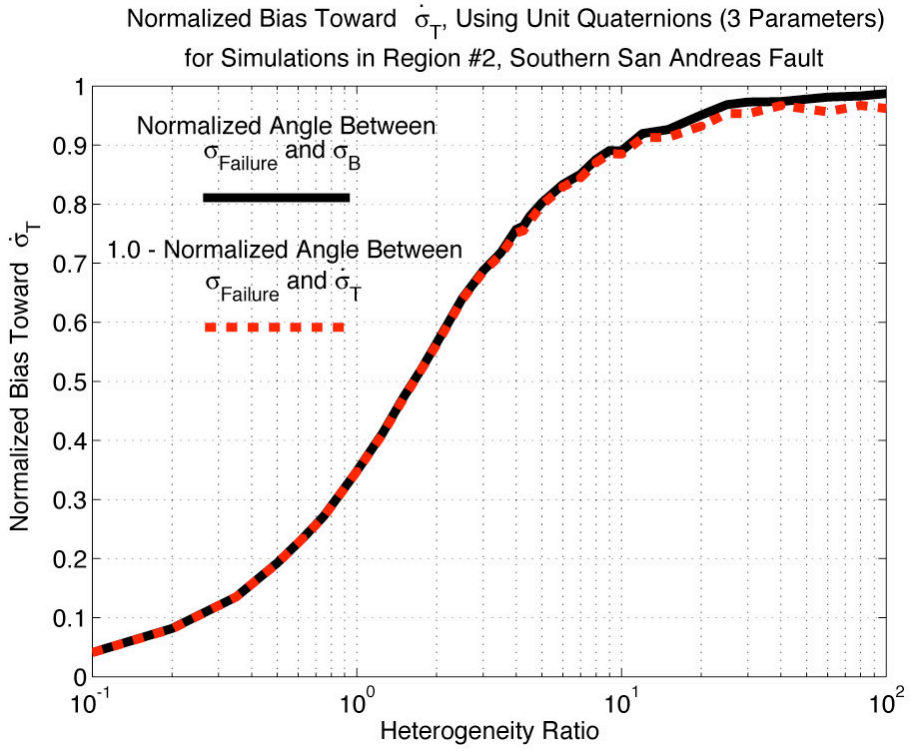

Figure 4.10 b)

Figure 4.10. *Exactly the same plots as Figure 4.9 except that the Normalized Bias is now being plotted instead of the angular Bias, where all the angles have been divided by the maximum possible angular difference,* $\angle\boldsymbol{\sigma}'_B\dot{\boldsymbol{\sigma}}'_T$. *The possible range of values is now* $0.0 \le \textit{Normalized Bias} \le 1.0$, *where the Normalized Bias is really the percent rotation toward the* $\dot{\boldsymbol{\sigma}}'_T$ *orientation.*

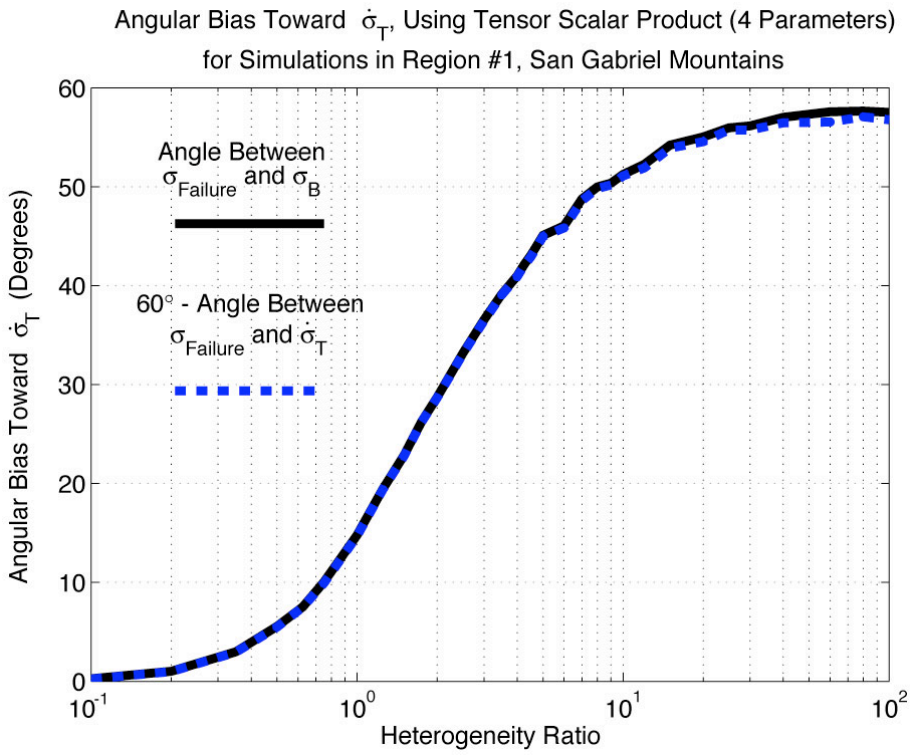

Figure 4.11 a)

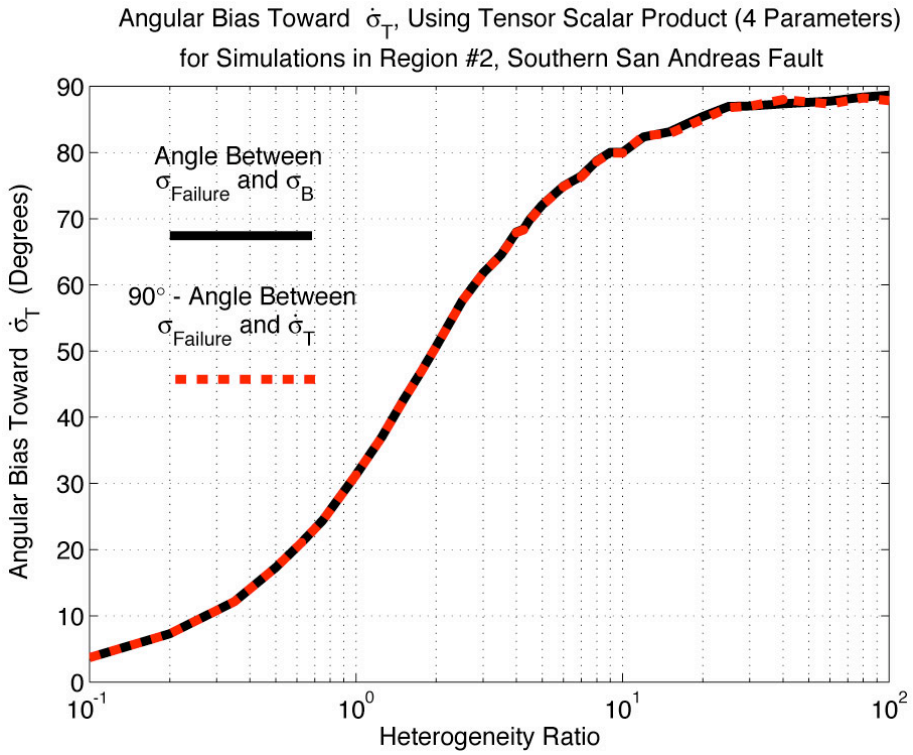

Figure 4.11 b)

Figure 4.11. *Plots of angular Bias toward the stressing rate orientation,* $\dot{\boldsymbol{\sigma}}'_T$*, as a function of heterogeneity ratio,* HR*, for the* ***a)*** *San Gabriel Mountains and the* ***b)*** *Southern San Andreas. Bias is calculated two different ways in this plot. The solid black line shows the angular difference between,* $\bar{\boldsymbol{\sigma}}'_{Failure}\left(\mathbf{x}_{i_{Failure}}, t_{Failure}\right)$ *and* $\boldsymbol{\sigma}'_B$*,* $\angle\bar{\boldsymbol{\sigma}}'_{Failure}\boldsymbol{\sigma}'_B$*, and the dashed red line, which plots almost exactly on top shows* $\angle\boldsymbol{\sigma}'_B\dot{\boldsymbol{\sigma}}'_T - \angle\bar{\boldsymbol{\sigma}}'_{Failure}\dot{\boldsymbol{\sigma}}'$*. The angular difference for these two quantities,* $\angle\bar{\boldsymbol{\sigma}}'_{Failure}\boldsymbol{\sigma}'_B$ *and* $\angle\boldsymbol{\sigma}'_B\dot{\boldsymbol{\sigma}}'_T - \angle\bar{\boldsymbol{\sigma}}'_{Failure}\dot{\boldsymbol{\sigma}}'$*, is calculated using our four-parameter method. This method takes the tensor scalar product of deviatoric stress matrices that have been calculated from the three principal stress orientations and the stress ratio,* R*, and calculates an angle. The red dashed line and the solid black lines are averages over simulations with three different levels of spatial smoothing,* $\alpha = 0.0$*,* $\alpha = 0.5$*, and* $\alpha = 1.0$*. In this figure, using the four-parameter method, both the Southern San Andreas Fault simulations and the San Gabriel Mountain simulations smoothly rotate from* $\boldsymbol{\sigma}'_B$ *to* $\dot{\boldsymbol{\sigma}}'_T$ *as* HR *increases, which is more desirable than the abrupt transition seen for the San Gabriel Mountains seen in Figure 4.9 using the three-parameter method. While the four-parameter method for calculating angular differences is by far the best, it can only be applied when one has an estimate of the stress ratio,* R*. If one has only orientation information, such as strike, dip, and rake* $(\Theta, \delta, \lambda)$ *when dealing with individual focal mechanism orientations, then one cannot use this four-parameter methodology.*

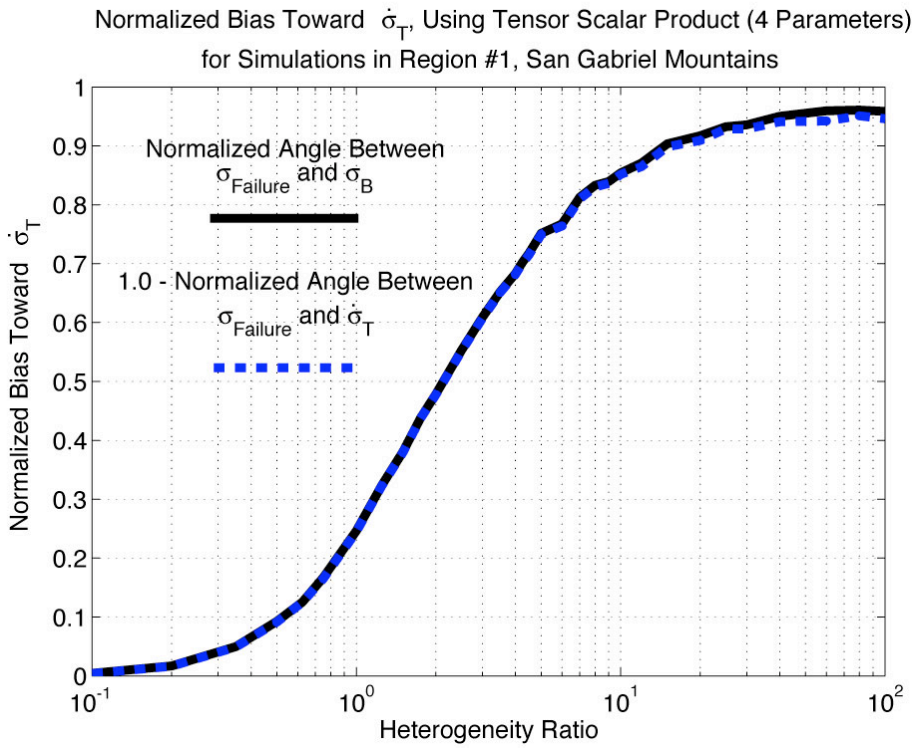

Figure 4.12 a)

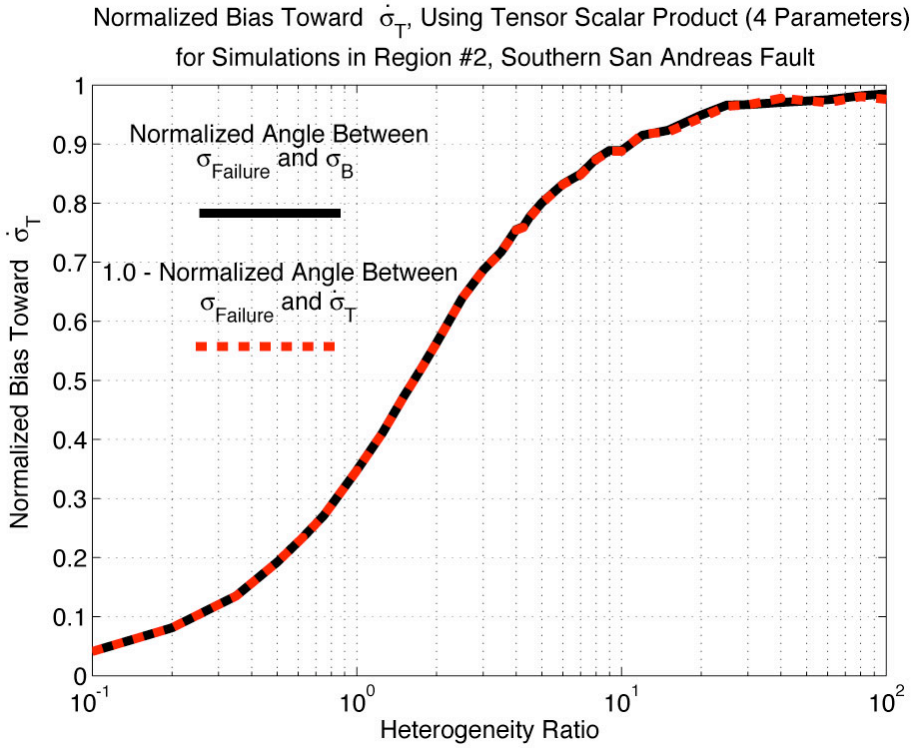

Figure 4.12 b)

Figure 4.12. *Exactly the same plots as Figure 4.11 except that the Normalized Bias is now being plotted instead of the angular Bias, where all the angles have been divided by the maximum possible angular difference,* $\angle \boldsymbol{\sigma}'_B \dot{\boldsymbol{\sigma}}'_T$. *The possible range of values is now* $0.0 \le Normalized\ Bias \le 1.0$, *where the Normalized Bias is really the percent rotation toward* $\dot{\boldsymbol{\sigma}}'_T$. *Note how similar are the Normalized Bias plots of the San Gabriel Mountains and Southern San Andreas as they both smoothly rotated toward* $\dot{\boldsymbol{\sigma}}'_T$ *using this four-parameter method of estimating angular differences.*

References

Angelier, J. (1975), Sur l'analyse de mesures recueilles dans des sites faillés: l'utilité d'une confrontation entre les méthodes dynamiques et cinématiques, *C.R. Acadamy of Science, Paris, D*, *283*, 466.

Angelier, J. (1984), Tectonic analysis of fault slip data sets, *Journal of Geophysical Research*, *89*, 5835–5848.

Carey, E., and B. Brunier (1974), Analyse théorique et numérique d'un modèle méchanique élémentaire appliqué à l'étude d'une population de failles, *C.R. Acadamy of Science, Paris, D*, *279*, 891–894.

Etchecopar, A., et al. (1981), An inverse problem in microtectonics for the determination of stress tensors from fault striation analysis, *Journal of Structrual Geology*, *3*, 51–65.
Gephart, J. W. (1990), FMSI: A Fortran program for inverting fault/slickenside and earthquake focal mechanism data to obtain the regional stress tensor, *Computers and Geosciences*, *16*, 953–989.

Gephart, J. W., and D. W. Forsyth (1984), An improved method for deteremining the regional stress tensor using earthquake focal mechanism data: Application to the San Fernando earthquake sequence, *Journal of Geophysical Research*, *89*, 9305–9320.

Housner, G. W., and T. J. Vreeland (1965), *The Analysis of Stress and Deformation*, 440 pp., Division of Engineering and Applied Science, California Institute of Technology.

Mercier, J.-L., and S. Carey-Gailhardis (1989), Regional state of stress and characteristic fault kinematics instabilities shown by aftershock sequence: the aftershock sequence of the 1978 Thessaloniki (Greece) and 1980 Campania-Lucania (Italy) earthquakes as examples, *Earth and Planetary Science Letters*, *92*, 247–264.

Michael, A. J. (1984), Determination of stress from slip data: Faults and folds, *Journal of Geophysical Research-Solid Earth*, *89*, 11517–11526.

Michael, A. J. (1987), Use of focal mechanisms to determine stress: A control study, *Journal of Geophysical Research-Solid Earth*, *92*, 357–368.

Rivera, L., and H. Kanamori (2002), Spatial heterogeneity of tectonic stress and friction in the crust, *Geophysical Research Letters*, *29*, art. no. 1088.

Townend, J., and M. D. Zoback (2004), Regional tectonic stress near the San Andreas fault in central and southern California, *Geophysical Research Letters*, *31*, L15S11, 11–15.